7-27-2018

Heat Flux Calculation of PDMS and Silica Aerogel Through Phosphor Thermometry

Makunda Aryal

HEAT FLUX CALCULATION OF PDMS AND SILICA AEROGEL THROUGH PHOSPHOR THERMOMETRY

by

Makunda Aryal

A thesis

Submitted in Partial Fulfillment of the

Requirement for the Degree of

Master of Science

Major: Physics

The University of Memphis

August 2018

DEDICATION

Dedicated to My Family

ACKNOWLEDGEMENT

First, I would like to thank my supervisor, Dr. Firouzeh Sabri for giving me an opportunity to understand this study and for all her guidance and continuous encouragement throughout this work. I would also like to thank Dr. Steve Allison for his invaluable support for this study. I would like to thank Dr. M. Shah Jahan and Dr. Xiao Shen for accepting my request to serve on my thesis faculty committee. Also, I am thankful to all my friends who helped me during this thesis.

Finally, I want to express my sincere gratitude to my family without which I could not have come this far.

ABSTRACT

Phosphor thermometry is an accurate, versatile, and rapid mechanism for inferring temperature information, remotely. The working principle of this technique is based on the different emission characteristics of thermographic phosphors which varies from compound to compound and depends on the specific electronic structure(s) of the phosphor under investigation. Either temporal or spectral composition of the emission characteristics can be used to determine the temperature of the surface that the phosphors are in contact with. In this work thermographic phosphors have been encapsulated in inert transparent or translucent polymers and the behavior of the phosphor-polymer composites was studied as a function of temperature. Silica aerogels and Sylgard184 were chosen for this study and an array of phosphor patches was created on both sides of each material in an off-axis manner. Both aerogels and elastomers are widely used as insulating material but mostly in passive form. Here, the feasibility of imparting sensing capabilities to these materials and potentially measuring heat flux is explored and characterized. Results showed that because of the scattering that occurs in the aerogel material the maximum material thickness that can be accessed by phosphor thermometry is limited to ~ 6 mm, with the setup used in this study. In the case of Sylgard184 an upper limit was not reached. Both up-converting and down converting phosphors were studied. Finally, the performance of thin flexible ceramic films as a thermal buffer was investigated and fully characterized.

TABLE OF CONTENTS

Chapter Page

List of Figures ix

1 Introduction 1

1.1 Introduction to thermometry 1

1.2 History of phosphor thermometry 3

1.3 Introduction to heat flux measurement techniques 4

1.4 Introduction to aerogels 5

1.5 Research aims 6

1.6 Thesis outline 6

2 Theory 7

2.1 Heat transfer and temperature of materials 7

2.2 Heat transfer in solids 7

2.3 Heat flux 8

2.4 Phosphor thermometry 11

2.5 Thermographic phosphors 12

2.5.1 Thermographic phosphor characteristics 13

2.6 Decay time analysis …. 13

2.7 Luminescence ……. 15

3 Materials and Methods 18

3.1 Synthesis and preparation of aerogel and elastomers samples 17

3.1.1 Sylgard184-La_2O_2S: Eu phosphor composite synthesis 19

3.1.2 Sylgard184-$Mg_3F_2GeO_4$: Mn phosphor composite synthesis 20

3.1.3 Silica aerogel-La_2O_2S: Eu phosphor composite synthesis 21

3.1.4 Silica aerogel-$Mg_3F_2GeO_4$: Mn phosphor composite synthesis 23

3.1.5 Sylgard184-upconverting phosphor composite synthesis 24

3.1.6 Imaging and microscopy 25

3.2 Sample for the high temperature ceramic experiment 26

3.2.1 Ceramic samples 26
3.2.2 Heat distribution assessment 26
3.2.3 Mechanical Testing 27
3.2.4 Thermal barrier behavior of ceramic 28
3.2.5 Sample to study luminescence at high temperature 28
3.3 Sample characterization and testing 29
3.3.1 Porosimetry measurement of silica aerogel 29
3.3.2 Thermal conductivity measurement of silica aerogel 29
3.4 Temperature dependent luminescence setup 29
3.5 Decay time calculation 32
4 Results 33
4.1 Characterization of silica aerogel 33
4.1.1 Pore size and surface area analysis of silica aerogel 33
4.1.2 Thermal conductivity 35
4.2 Temperature dependent Luminescence of Composites 35
4.2.1 Calibration of La_2O_2S: Eu and $Mg_3F_2GeO_4$: Mn decay behavior 35
4.2.2 Temperature dependent luminescence of Sylgard184-La_2O_2S: Eu composite 36
4.2.3 Temperature dependent luminescence of Sylgard184-$Mg_3F_2GeO_4$: Mn composites 41
4.2.4 Temperature dependent luminescence of silica aerogel-La_2O_2S: Eu composites 42
4.2.5 Temperature dependent luminescence of silica aerogel-$Mg_3F_2GeO_4$: Mn composites 45
4.2.6 Emission behavior from neighboring phosphor patches 47
4.3 Heat flux calculation 48
4.4 Luminescence of upconverting phosphor 50
4.5 Microscopy images 52
5 Results: Temperature Dependent Luminescence of Flexible Ceramic Ribbons 56

5.1 Effect of ceramic ribbons on heat distribution 56
5.2 Flexural strength of ceramic ribbons 61
5.3 Heat distribution assessment on the ceramic sheet 62
5.4 Temperature dependent luminescence 63

6 Conclusion and Future Recommendation 66

References 68

LIST OF FIGURES

Figure Page

2.1 One-dimensional heat flux sensor....10

2.2 Schematic diagram of circular heat flux gage....11

2.3 Jablonski energy level diagram showing fluorescence and phosphorescence....16

3.1 Flow diagram showing the types of samples prepared....17

3.2 Schematic diagram of (a) pattern sample (b) Sylgard184 upconverting phosphor sample....18

3.3 Sylgard184-La_2O_2S: Eu phosphor composite having a thickness (a) 3.7 mm (b) 8.0 mm and (c) 12.0 mm....20

3.4 Sylgard184-$Mg_3F_2GeO_4$: Mn phosphor composite having a thickness (a) 4 mm and (b) 8.0 mm....21

3.5 Silica aerogel sample with La_2O_2S: Eu phosphor having a thickness (a) 2.2 mm and (b) 6.5 mm....23

3.6 Silica aerogel-$Mg_3F_2GeO_4$: Mn phosphor composite having a thickness (a) 2.2 mm and (b) 6.3 mm....24

3.7 Sylgard184 with 15 % of (a) Y_2O_2S:Er^{3+} Yb^{3+} phosphor composite (b) La_2O_2S: $Er^{3+}Yb^{3+}$ phosphor composite....25

3.8 Location of points taken on a ceramic sheet....27

3.9 (a) Schematic diagram of test setup and (b) actual setup of experiment....31

3.10 Flowchart diagram of temperature calculation....32

4.1 The adsorption and desorption isotherm of silica aerogel synthesized for this study....33

4.2 Pore diameter distribution of silica aerogel in BJH desorption model....34

4.3 Calibration of (a) La_2O_2S: Eu and (b) $Mg_3F_2GeO_4$: Mn phosphors over the temperature range of interest....36

4.4 Graph of stage temperature vs. decay time of Sylgard184 samples containing La_2O_2S: Eu phosphor patch arrays with thicknesses (a) 3.7 mm, (b) 8 mm, and (c) 12 mm....37

4.5 Graph of stage temperature vs. calculated temperature of Sylgard184- La_2O_2S: Eu composites for (a) 3.7 mm, (b) 8 mm and (c) 12 mm....39

4.6 Graph of stage temperature vs. calculated temperature difference (ΔT) between the top and the bottom surface of Sylgard184- La_2O_2S: Eu composites for (a) 3.7 mm, (b) 8 mm and (c) 12 mm thick sample....40

4.7 Graph of stage temperature vs. decay time of Sylgard184 samples containing $Mg_3F_2GeO_4$: Mn phosphor patch arrays with thicknesses (a) 4 mm and (b) 8 mm 41

4.8 Graph of stage temperature vs. calculated temperature difference (ΔT) between the top and a bottom surface of Sylgard184- $Mg_3F_2GeO_4$: Mn composites for (a) 4 mm and (b) 8 mm thick sample 42

4.9 Stage temperature vs. decay time of silica aerogel containing La_2O_2S: Eu phosphor patch arrays with thicknesses (a) 2.2 mm and (b) 6.5 mm 43

4.10 Stage temperature vs. calculated temperature of silica aerogel- La_2O_2S: Eu composites for (a) 2.2 mm and (b) 6.5 mm 44

4.11 Stage temperature vs. calculated temperature difference (ΔT) between the top and the bottom surface of silica aerogel- La_2O_2S: Eu composite for (a) 2.2 mm and (b) 6.5 mm samples 44

4.12 Stage temperature vs. decay time of silica aerogel containing $Mg_3F_2GeO_4$: Mn phosphor patch arrays with thicknesses for (a) 2.2 mm and (b) 6.5 mm 46

4.13 Stage temperature vs. calculated temperature of the top and a bottom surface for silica aerogel- $Mg_3F_2GeO_4$: Mn composites for (a) 2.2 mm and (b) 6.5 mm 46

4.14 Multipoint decay time vs. stage temperature for 8 mm Sylgard184- $Mg_3F_2GeO_4$: Mn composite 47

4.15 Heat flux vs stage temperature for aerogel- La_2O_2S: Eu and Sylgard184- La_2O_2S: Eu composites 49

4.16 Fluorescence signal vs time and normalized signal vs time for decay curve (inset) for (a) Y_2O_2S: Yb, Er in Sylgard184 and (b) La_2O_2S: Yb, Er in Sylgard184 50

4.17 Normalized fluorescence rises signal vs time for (a) La_2O_2S: Yb, Er in Sylgard184 and (b) Y_2O_2S: Yb, Er in Sylgard184 51

4.18 SEM images of (a)La_2O_2S: Eu and (b) $Mg_3F_2GeO_4$: Mn (c) Y_2O_2S: Er, Yb and (d) La_2O_2S: Er, Yb 52

4.19 Surface roughness images of (a) Sylgard184 surface, (b) phosphor surface on Sylgard184 and (c) Sylgard184 phosphor boundary 53

4.20 Surface roughness image of (a) aerogel surface, (b) phosphor surface on aerogel and (c) aerogel phosphor boundary 54

5.1 Graph of the number of ceramic layer vs. change in temperature (ΔT) due to ceramic layers for Sylgard184. Error bars reflect the standard deviation 57

5.2 Graph of the number of ceramic layer vs. change in temperature (ΔT) due to ceramic layers for silica aerogel. Error bars reflect the standard deviation 58

5.3 UV-Vis graph (a) % transmission (% T), (b) absorbance (A) for Sylgard184 and, (c) % transmission (% T), (d) absorbance (A) for silica aerogel 60

5.4 Flexural Strength: Force (F) vs. displacement (d) graph of the ceramic ribbons 61

5.5 Graph showing the temperature distribution on the ceramic sheet.....63

5.6 Plot of (a) signal voltage with time (b) log of signal voltage with time to find decay time of Gd_2O_2S: Eu/ceramic composite and (c) signal voltage vs time with a regression fit for YAG: Dy-ceramic composites at 1039 ^0C.....64

Chapter 1

Introduction

1.1 Introduction to thermometry

Surface temperature measurement is especially crucial for the determination of heat transfer as well as for many industrial processes and monitoring tasks [1]. Temperature measurements can be conducted in a variety of ways and the method chosen will depend on the application and the resolution that is needed for that particular application. Resistive temperature detector phase changing temperature labels and optical pyrometry are examples of thermometry instruments and each has its limitation. For example, thermocouples need a direct thermal contact (contact based), which is difficult to achieve in some applications and circumstances [2]. In order to use the pyrometry technique for thermometry the emissivity of the surface is required and using this is limited where the emissivity varies with time [3]. In the case of temperature labels, the encapsulated liquid crystal has a slow response time and as a result temperature labels are not reliable for rapid and accurate temperature reading with a high degree of resolution.

The phosphor thermometry technique, on the other hand, is a very reliable, accurate, and remotely detectable temperature sensing method that is superior to the methods mentioned above [4]. The thermal dependence of phosphor fluorescence may be exploited to provide for a non-contact, emissivity independent, optical alternative to other more conventional techniques, e.g., those employing pyrometry, thermocouples, or thermistors. In fact, there are certain situations in which the advantages fluorescence-based thermometry has over other methods make it the only useful approach. Phosphor thermometry is a non-contact, optical, instantaneous and precise

method of measuring the temperature of the intended surface or object. This method is suitable for a wide range of temperatures from cryogenic to 2000 ^{0}C in some cases [5]. Thermographic phosphors are rare earth-doped ceramics that fluoresce when exposed to light. The temperature sensitive behavior of a phosphor can provide a viable means of monitoring the temperature profiles of surfaces and also measuring the temperature in a variety of situations. The emission wavelength, intensity, and decay rate are all temperature dependent, so any of these properties can be measured to determine temperature. This method is good for surface temperature measurements and proven to be useful and accurate for a variety of thermal measurement applications [5], [6]. Usually, phosphorescence decay time, also known as lifetime, is the parameter that is measured to determine the temperature. This technique offers high sensitivities and accuracies [5].

In the past, most phosphor thermometry applications have focused on utilizing these compounds in powder form and this has seriously limited its range of application due to complications associated with using fine powders. The focus of this research has been to investigate methods to reliably incorporate thermographic phosphors in a polymeric encapsulant without interference with or modification of the excitation –emission characteristics of the phosphors. The two polymers that were chosen for this study include transparent elastomers that are commercially available, Sylgard184, and silica aerogels. Sylgard184 is of the polydimethylsiloxane (PDMS) family. It is an optically clear, inert material and can be used widely in various studies including biomedical, optical and aerospace application [7]. The polymer from this family has versatile nature so that it can be used as fine tuning of bulk as well as surface properties for different application [8].

Luminescence refers to the absorption of energy by a material, with the subsequent emission of light. This is a phenomenon distinct from blackbody radiation, incandescence, or other

such effects that cause the material to glow at high temperature. Fluorescence refers to the same process as luminescence, but with the qualification that the emission is usually in the visible band and has a duration of typically 10^{-9} to 10^{-3} s. Phosphorescence is a type of luminescence of greater duration, $\approx 10^{-3}$ to 10^{3} s [9].

1.2 History of phosphor thermometry

The study of phosphor thermometry was begun in 1938 after the development of fluorescence lamp [10]. Initially, phosphors were used for domestic lighting and making cathode ray tubes. When used as light sources, investigators found the degradation of brightness at a higher temperature. Therefore, they started to study its thermal and optical properties. Neubert suggested the use of phosphor for thermometry in 1937 [11]. The first use of this technique to find temp was in 1952 by Bradley [12] who measured the temperature distribution on a flat wedge in supersonic flow. Later on, in 1979, James et al found out decay time characteristics of phosphor which are temperature dependent [13]. In the decade of 1980's significant progress was made in phosphor thermometry by the advent of the short pulse laser. Later, for example, Tobin et al [14] showed the successful use of this technique to find the surface temperature of the rotating systems. Allison et al showed its use in aerospace application [15]. Also, Omrane demonstrated this technique to measure the temperature of flame [16]. It is used in scientific and industrial applications of surface thermometry to complicated geometries, e.g., rotor engines, turbines engines[17]. During the recent years, as the applications of thermographic phosphors have expanded, some attempts have been made in the combustion environment [18].

1.3 Introduction to heat flux measurement techniques

Precise measurements of the temperature of surfaces can be particularly important when designing and building instrumentation for evaluating heat flux. Examples of heat flux instrumentation include work published by Diller et al [19] where a heat flux gauge was built using thin film layers on each side of the thermally insulating material with its cold junction applied to one surface and hot junction to other surfaces. These thin films allow the deposition of a large number of junctions onto a small area which generates electrical resistances and its needs wire connections for measurement.

Epstein et al. [20] use the double-sided high-frequency response heat flux gauge. This gauge consists of 1500 Angstrom thin metal film applied to 25- μm thin polyimide sheet on both sides. At low frequency, the heat flux is obtained by the direct measure of the temperature difference between two sides of a polyimide sheet. At higher frequency, a quasi-one-dimensional assumption is used to find heat flux. Another heat flux gauge was disclosed by Hayashi et al. [21] where a pair of metallic thin films are attached to the opposite sides of heat resistive thin film. Heat flux is measured by measuring the temperature gradient between heat resistive film using the metallic thin films resistance thermometer.

All the techniques mentioned above are electrically based, require wire connections and, are contact based which once again limit their range of applications and their accuracy and response time. These issues and technical concerns were partially overcome by Noel et al. [22] who proposed a different technique to measure heat flux. They used thermographic phosphor as a temperature sensor for calculating heat flux. In their case thermographic phosphors were deposited on both sides of thermally insulating materials and using the optical properties of the emission of

phosphor they calculated heat flux. In this technique, they used two different types of phosphor on two sides of the material to distinguish the emitted signals between the top and bottom.

The research presented here follows what Noel et al. have done and aerogels and elastomers serve as the insulative medium.

1.4 Introduction to aerogels

Aerogel, first introduced by Kistler in 1931, is a mesoporous ultralight material prepared by means of the sol-gel method in which the liquid component of the gel is replaced with a gas in a supercritical dryer. NASA used aerogels to capture micron sized space dust in Space Shuttle experiments [23]. Aerogels have been found to exhibit some of the lowest thermal conductivities among all solids [7]. This is because of the unique nanostructure of the aerogel which forces the heat to travel through a very narrow labyrinth chain of the solid skeleton to reach the other side. Various types of aerogel have been synthesized over the years but the core nanoparticles of most of the aerogel consist of silica and are among the most studied variety of aerogels. The demand for aerogels as an insulator and interest in understanding it's properties continues to grow and is under investigation by many industries [24], [25]. Given that in the majority of cases aerogels are investigated to serve as high performing insulation for extreme conditions, the exact distribution of heat and flow of thermal energy across the material is of key importance and critical to the safety and operation of the material. Therefore, accurate investigation and understanding of the temperature of the aerogels is essential. In this work, I have investigated the methods to incorporate temperature sensing capabilities in aerogels and will report on all results related to this investigation. The study is conducted in parallel with an investigation of and fully characterized

over a wide temperature range transparent elastomer and, flexible ceramic sheets. The performance of these materials are compared.

1.5 Research aims

The purpose of this research is listed below.

- Creating the phosphor patterned in Sylgard184 and silica aerogel
- Studying the luminescence behavior of different types of phosphor in such a pattern.
- Introducing the sensing mechanism in silica aerogel
- Studying the emission properties of the upconverting phosphor

1.6 Thesis outline

This thesis is organized in the following manner:

Following this chapter, Chapter 2 will describe the theory behind luminescence, concepts, and mechanism of heat transfer in solids, and the physics behind phosphor thermometry. All methods related to sample preparation and characterization of the compounds and composites prepared will be presented in Chapter 3. All results from characterization efforts and measurements are presented in Chapter 4. The work related to thermometry with thin ceramic sheets is given in Chapter 5. Finally, Chapter 6 gives the conclusion of this work with future recommendations.

Chapter 2

Theory

2.1 Heat transfer and temperature of materials

Heat is the total kinetic energy of the molecules in the substances. Whereas temperature is the average kinetic energy. Thermal energy is related to the temperature and the higher the temperature, the higher will be the thermal energy of a body. Heat transfer is the exchange of thermal energy due to the temperature difference between bodies or throughout the body [26]. When the two bodies are at different temperature then there is always the transfer of heat. The transfer takes place from higher temperature to lower temperature There are three basic mechanisms of heat transfer. These are (1) conduction, (2) convection and (3) radiation. It is assumed here that the dominating mode of heat transfer in solids is conduction and is discussed further below:

2.2 Heat transfer in solids

Conduction is the basic mechanism of heat transfer in solids and stationary liquids. There are two phenomenon which explains how heat transfer in solids. One is lattice vibration and other is the particle collision. Atoms are bound with each other by bonds in solid. When there is a temperature difference between solids then the atom on the hotter side experiences more vibration. This vibration is then transferred to the cooler side. In this way, there is the transfer of thermal energy by collision. Another mechanism is that the metal consists of free electrons which are not

bound and are free to move. So, free electrons play a role to transfer heat energy from one point to another. The electron in the hotter side move faster and transfer energy to the cooler side [27].

2.3 Heat flux

Heat flux is determined as the amount of heat transferred through the unit of area in a unit of time. Heat flux measurements are necessary for areas where the measurement of an energy transfer is favored over the temperature measurement. Such need can be found in industrial process control or electrical machines. Surface temperature measurements techniques such as a thermocouple, infrared thermography, and thermal paints are used in conjunction with heat transfer model to calculate heat flux. The measurement accuracy of heat flux is highly related to the accuracy of surface temperature measurements.

The Fourier's law relates the temperature distribution with heat flux. Which states that the heat flux vector is proportional to and in the opposite direction of the temperature gradient [1]. The Fourier' law is given below.

$$q = -k\nabla T \tag{1}$$

Here, q = heat flux

K = thermal conductivity

∇T = temperature gradient

In a one-dimensional form, the Fourier's law is written as

$$q = -k\,\frac{dT}{dX} \tag{2}$$

Where, q = heat flux

k = thermal conductivity

dT = difference in temperature

dx = Thickness

The heat flux q is a vector quantity. The minus sign shows that the heat flows from the hotter part to the colder part. The thermal conductivity k is the property of the material. It is defined as the ability of the material to conduct heat.

Heat flux sensors are used to measure the rate of heat flow in many applications. For example, heat flow measurements through walls, clothing, human skin, insulation material and so on. There arethree heat flux sensing approaches [1]. They are heat flux based on surface heating, temperature change with time and heat flux based on a temperature gradient. Here, in our experiment, we are studying heat flux based on temperature gradient approach.

There are various types of commercially available heat flux gauge and sensors. These sensors have certain advantages in a particular situation. Most of these sensors use thermocouple for temperature determination.

(i) One dimensional planar sensor

This is the simplest heat flux sensor and the concept of this is illustrated in Figure 2.1. The following equation is used in this one-dimensional planar sensor.

$$q = \frac{k}{d}\,(T_1 - T_2) \qquad (3)$$

Here, q = one-dimensional heat flux, k is thermal conductivity of sample and d is the thickness of sensors. In this case, as shown in Figure 3.1, two temperature sensors are used on top and bottom of the sample. An adhesive layer may also be required between the temperature sensors and sample

surface to attach sensors on surfaces. Thermocouples are used as temperature sensors. Although, thermocouples are widely available and easy to use theysuffer many disadvantages for some applications. Also, the adhesive layer may also add some thermal resistance and increase thermal disruption. So, we cannot use this type of sensor with greater accuracy.

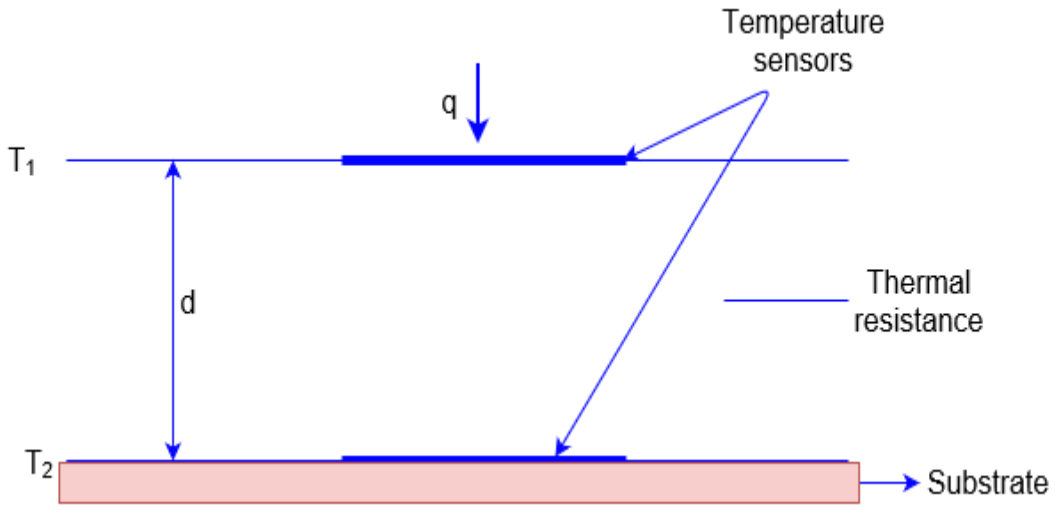

Figure 2.1: One-dimensional heat flux sensor [1]

(ii) Circular foil gage

This sensor is also known as Gardon gauge. This gage consists of a hollow cylinder of one type of thermocouple material in which a circular foil of another type of thermocouple material is attached at one end. A wire made of first thermocouple material is attached to the center of circular foil which makes thermocouple pair between the center of foil and edge. This thermocouple pair measures the temperature difference between the center and edge of foil. Generally, this type of gauge is used to measure radiation heat transfer [28]. In this gage, the circular foil is usually made up of constantan and another is made from copper. For a uniform heat flux case, the heat

flux is proportional to the temperature difference between edge and center of foil. The schematic diagram is shown in Figure 2.2 [19].

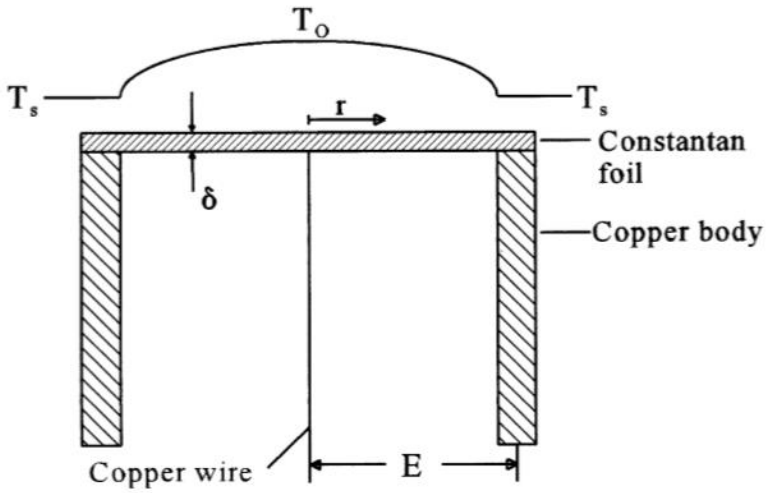

Figure 2.2: Schematic diagram of a circular heat flux gage [1]

The equation to find heat flux is given below

$$T_0 - T_s = \frac{qR^2}{4k\delta} \quad (4)$$

Here, T_0 is the temperature at the center of foil, T_s is at the edge of the foil, R is the radius of circular foil, k is thermal conductivity, δ is the thickness of foil and q is heat flux.

2.4 Phosphor thermometry

Phosphor thermometry uses thermographic phosphor as the sensing material to calculate the temperature. The phosphors are called thermographic if one or more characteristic depends upon temperature change. It is an optical and remote technique. It uses the optical signal generated from the thermographic phosphor to determine the temperature profile of the material. In this technique, phosphors are incorporated into the materials of interest. Several of its features make phosphor thermometry an attractive technique of surface temperature measurements. Temperature

can be measured anywhere on the coated surface rather than at a point location. The particular advantage comes from the robustness and stability of the phosphor materials used whose melting temperature is above 2000 ^{0}C. This enables phosphor thermometry to use at a very high temperature as well as harsh environment also.

2.5 Thermographic phosphors

The phosphor which is specifically designed to measure the temperature is called thermographic phosphor. They are generally white or lightly colored. Based on their composition, they are divided into two parts: organic and inorganic phosphor. The inorganic phosphors are used especially for high temperature applications because they survive high temperature. Phosphor consists of two components one is host matrix which may be a ceramic and the other is activator atom. The host compound is highly homogeneous and stable at high temperature also. while the activator is rare earth or transition metal ion. This forms a very complex system. Each component exhibits their own energy levels resulting in a large number of electronic transition is possible. The excitation energy is absorbed either by the host or activator atom. In return to ground state, a number of radiative and non-radiative transition takes place. All these transitions are affected by temperature. From this phenomenon, the temperature dependence of luminescence comes from. The normally available particle size of the phosphor is in the range of 1 to 10 μm. Thermographic phosphors are excited with an energy source such as an electron beam, UV light, or a voltage source, and the emitted luminescence can be in the UV, visible, or even in the infrared region [5].

2.5.1 Thermographic phosphor characteristics

Various emission characteristics of thermographic phosphors have been utilized for thermometry applications [29]. The emission characteristics are listed below.

(i) Decay time analysis

(ii) The ratio of intensity lines

(iii) Rise time analysis

(iv) Absorption of excitation wavelength

(v) Emission line shift and line width analysis

In our work, we are utilizing temperature sensitive decay time characteristics of emission. Various studies have shown that this decay time method gives higher measurement precision [30] [31].

2.6 Decay time analysis

The most common method used to determine the temperature of a surface is the luminescent lifetime. Most of the time phosphors are downconvertors. For downconvertors, the source wavelength is shorter than the emitted fluorescence. The luminescence intensity decays exponentially according to the relation [32].

$$I = I_0 e^{-t/\tau} \qquad (5)$$

where I is the intensity, I_o is the initial intensity, t is the time, and τ is the decay time constant. The temperature dependence of the lifetime arises from the probability of each state being occupied at different temperatures. The number of non-radiative transitions increases at high temperatures compared to lower temperatures. Therefore, decay times are much shorter at high temperatures

since more of the luminescent energy is being converted to phonon emission instead of luminescent energy.

Eq. 5 can be written as

$$\frac{I}{I_0} = e^{-t/\tau}$$

$$\ln\left(\frac{I}{I_0}\right) = -t/\tau \qquad (6)$$

Comparing Eq. (6) with y = mx + c, the equation of straight line, $-1/\tau$ is the slope. Hence the reciprocal of the slope gives decay time.

The following phosphors are used in the experiments.

(i) Lanthanum oxysulphide doped with europium (La_2O_2S: Eu)

The La_2O_2S: Eu has sharp emission lines. The emission lines are located at 512nm, 538 nm, and 624 nm. These three emission lines are usually used for decay time phosphor thermometry. All these emission lines have different working temperature range. This phosphor gives luminescence decay curve from cryogenic temperatures [33] to 600 K. This phosphor has excellent sensitivity near room temperature. The sensitivity of 538 nm emission line lies between 350 K to 625 K. The 512 nm has sensitivity in the lower temperature and 624 nm in the higher temperature than 538 nm line. In this case, the optical transition occurs between 5D and 7F bands of the Eu^{3+} doping agent.

(ii) Manganese activated magnesium flurogermanate ($Mg_3F_2GeO_4$: Mn)

The temperature can be obtained from decay time analysis as well as intensity ratio method by using this phosphor. This phosphor has wide temperature sensitivity from 293 K to 1070 K. The sensitivity is greatest above 650 K. This can also be used at

cryogenic temperature [34]. The different gas atmosphere does not affect the emission behavior of this phosphor up to 10 bars of pressure [35]. The F atom in the phosphor increases the emission efficiency by 3 times [36]. However, the emission from the luminescence center of Mn^{4+} is temperature dependent [37].

(iii) Yttrium oxysulphide doped with ytterbium, erbium (Y_2O_2S: Er, Yb) and lanthanum oxysulphide doped with ytterbium, erbium (La_2O_2S: Yb, Er).

These phosphors are double doped and are called upconverting phosphor. Upconversion is the process in which the electron absorbs two or more than two photons with a lower energy usually in the IR region and emits a single photon with higher energy in the visible region [38]. This phosphor can be used as IR radiation detection. The phosphor with host material Y_2O_2S has attractive properties like insoluble to water, chemically stable, high melting point and low phonon energy. These upconverting phosphor can be used in biomedical diagnosis, display screen, and medical imaging.

2.7 Luminescence

A hot body that emits radiation solely because of its high temperature emits blackbody radiation. Luminescence is also the phenomenon of emission of light but not due to high temperature. All other forms of light emissions are called luminescence. It is also called cold emission of light. Researchers have observed many types of luminescence like bio-luminescence, photoluminescence, and chemoluminescence. Here, we are using light source as an excitation, so we are studying photoluminescence.

Luminescence is formally divided into two categories: fluorescence and phosphorescence [39] based on the nature of the excited state. Sometimes these two terms can be used interchangeably. The only difference between the two-term is a lifetime. Phosphoresces has a longer lifetime than fluorescence. In excited singlet state, the electron in the excited orbital is paired with the opposite spin of the electron to ground state so the transition is spin-allowed and occurs rapidly by the emission of light. Which is the fluorescence and typically the life is 10^{-9} s. On the other hand, the emission of light from the triplet excited state in which the electron has the same spin to the ground state is phosphorescence. Transition to the ground state is forbidden and hence the emission rate is slow so that phosphorescence's lifetimes are typically milliseconds to seconds [39].

In general, excitation causes the energy of luminescent molecules to jump to higher electronic states. This configuration state is not permanent; vibrational relaxation, internal conversion, intersystem crossing and emissions soon follow, resulting in the excited state returning to the ground or an intermediate state. This process can be summarized with a Jablonski energy-level diagram [40].

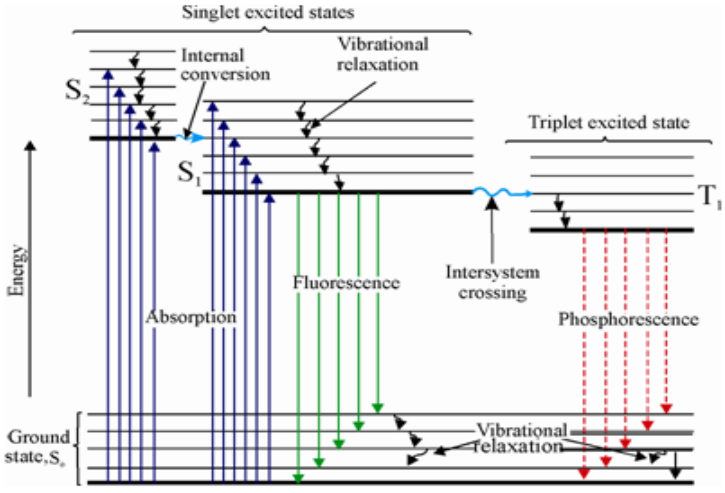

Figure 2.3: Jablonski energy level diagram showing fluorescence and phosphorescence [41]

Chapter 3

Materials and Methods

This chapter contains a detailed overview of the types of samples prepared for this study and, all experimental methods and techniques used to characterize the prepared samples. This chapter also gives a detailed description of how temperature dependent luminescence was evaluated. All downconverting phosphor powders used in this study were acquired from Phosphor Technology, UK. Upconverting phosphors were acquired from Intelligent Materials in powder form. Finally, flexible ceramic ribbons of 40 µm width were acquired from ENrG Inc. Figure 3.1 summarizes the types of the sample prepared in this study and is described in detail in the section below.

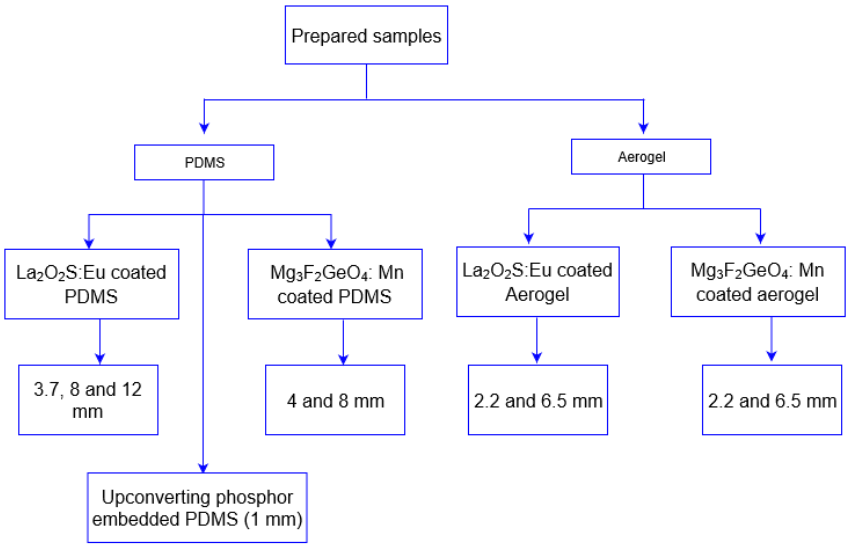

Figure 3.1: Flow diagram showing the types of samples prepared

3.1 Synthesis and preparation of aerogel and elastomers samples

Different types of Sylgard184-phosphors and native silica aerogel/phosphors composites with increasing thicknesses were prepared. In one sample design, an array of phosphor dots was patterned on both sides of the sample in an off-axis position. A schematic diagram is shown in Figure 3.2 a. This consists of the Sylgard184 with lanthanum oxysulphide doped with europium whose lot number is 23015 (La_2O_2S: Eu) and manganese activated magnesium flurogermanate with lot number 23145 ($Mg_3F_2GeO_4$: Mn). The phosphor used was from Phosphor Technology and Sylgard184 from Dow Corning. Also, silica aerogel with both phosphor types was prepared. The purpose of having an off-axis pattern is to excite phosphor via a light emitting diode (LED) and to detect signals without obstructing it on both sides of the sample.

On the other hand, Sylgard184 phosphor composite with upconverting phosphor was prepared. In this case, the upconverting phosphor was mixed with Sylgard184. The luminescence behavior of this upconverting phosphor Sylgard184 composite was investigated. The schematic diagram is shown in Figure 3.2 b.

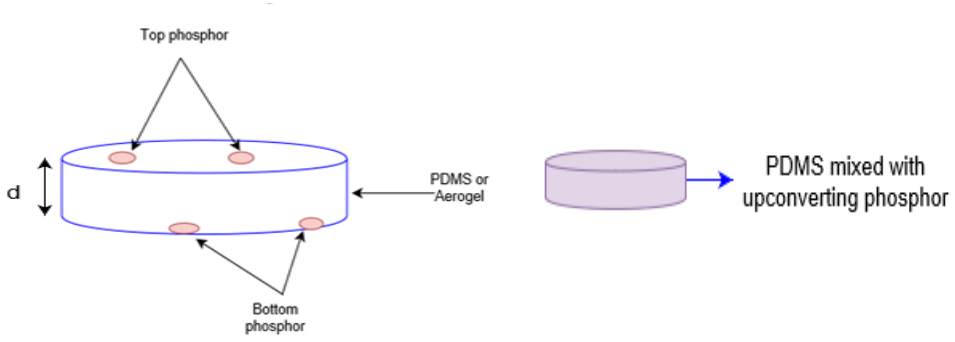

(a) (b)

Figure 3.2: Schematic diagram of (a) pattern sample (b) Sylgard184 upconverting phosphor sample

3.1.1 Sylgard184-La_2O_2S: Eu phosphor composite synthesis

Sylgard184 silicone elastomer base and curing agent were weighed in Fisher XE series 100A microbalance and were mixed in the ratio of 10:1 and then stirred thoroughly. The mixture was then outgassed in a Precision model 19 vacuum oven until all air bubbles were removed. After that, a dot pattern of La_2O_2S: Eu powder was put in a bottom of boat and mixture was poured over it for the desired thickness. For the top pattern, La_2O_2S: Eu powder was added in an off-axis pattern. In this way, Sylgard184 was sandwiched between the alternate dot patterns of La_2O_2S: Eu powder. At the end of the process, it was cured in Cascade Tek vacuum oven at 70 ^oC for 1 hours. Finally, samples were tested using 3-M tape to ensure good adhesion between the powder and the substrate and no phosphor particles were detached from the base. Enough powder was used to make that spot opaque. Three different sample thicknesses were prepared: d=, 3.7 mm, 8 mm and 12 mm.

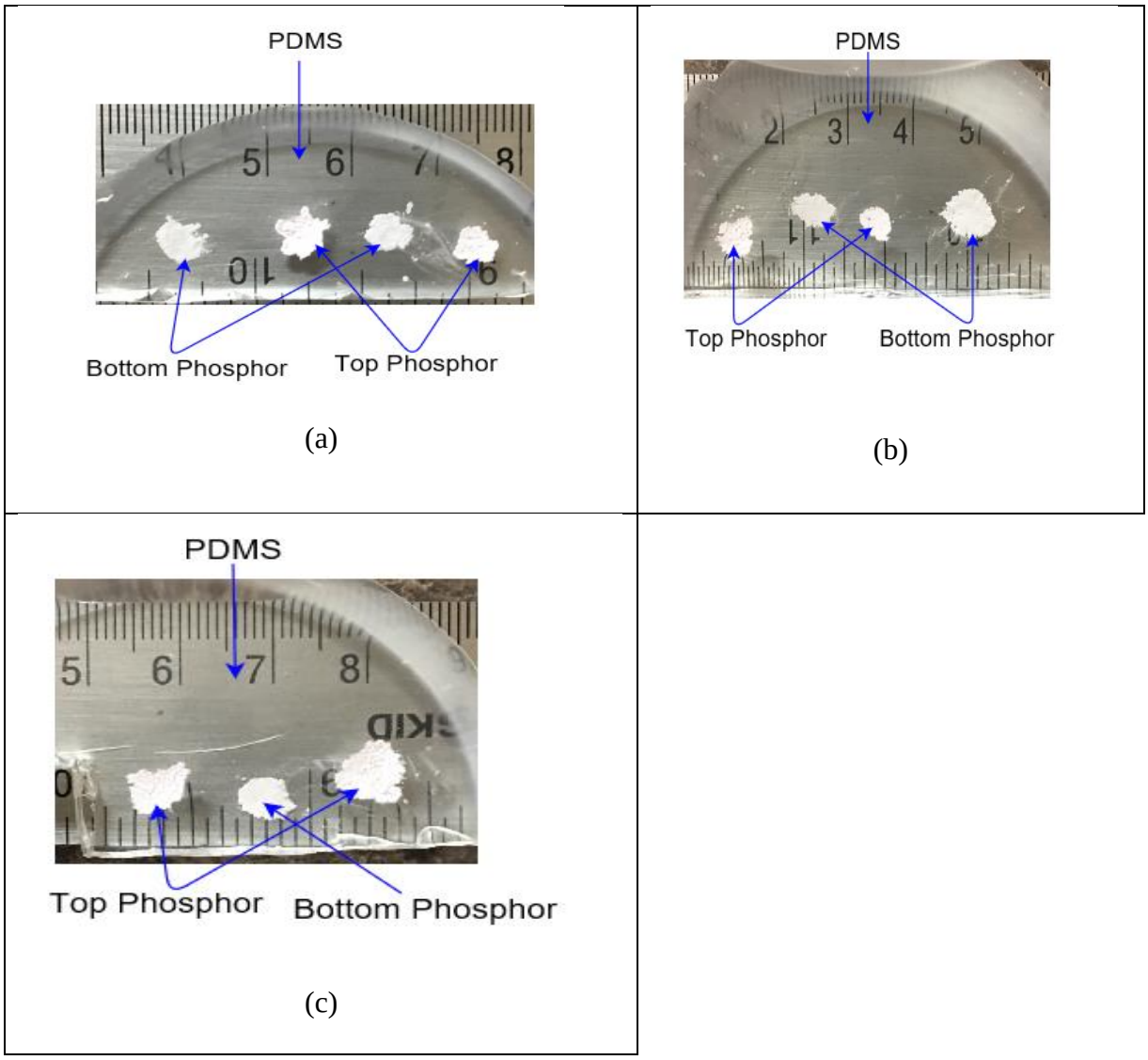

Figure 3.3: Sylgard184-La_2O_2S: Eu phosphor composite with thicknesses (a) 3.7 mm (b) 8.0 mm and (c) 12.0 mm

3.1.2 Sylgard184-$Mg_3F_2GeO_4$: Mn phosphor composite synthesis

To make this sample type, the same method as described in section 3.1.1 was used but with $Mg_3F_2GeO_4$: Mn phosphor instead of La_2O_2S: Eu phosphor. 4 mm and 8 mm thick samples were prepared.

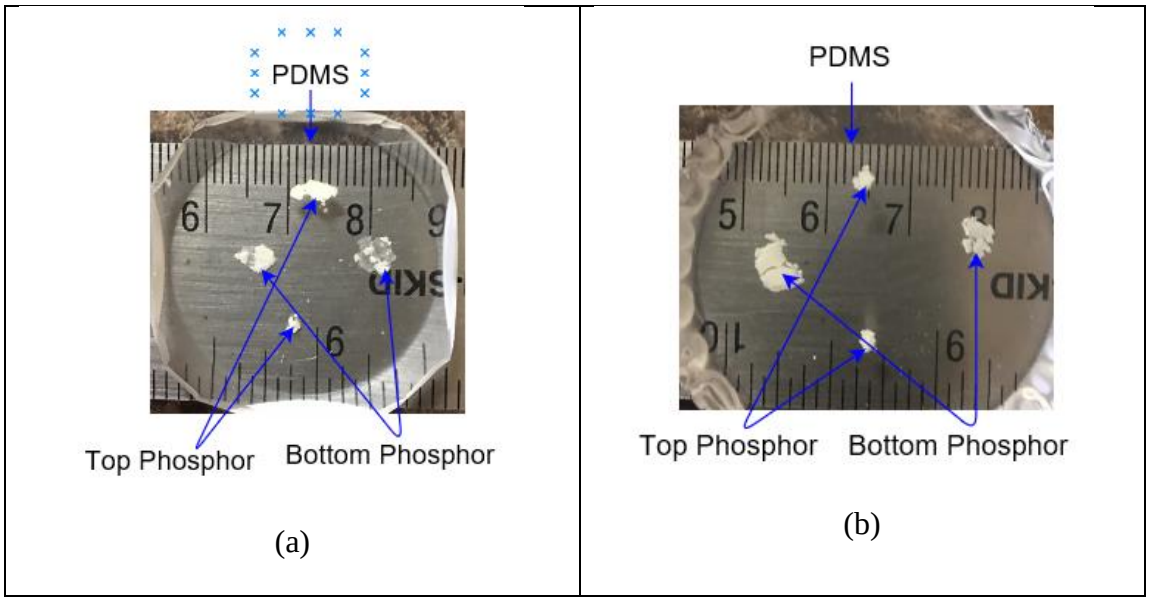

Figure 3.4: Sylgard184-$Mg_3F_2GeO_4$: Mn phosphor composite having a thickness (a) 4 mm and (b) 8.0 mm

3.1.3 Silica aerogel-La_2O_2S: Eu phosphor composite synthesis

4.25 mL of methanol was taken in a beaker A. Another 4.5 mL of methanol was mixed with 1.5 mL of deionized water and was put in beaker B. 3.85 mL of tetramethoxysilane (TMOS) was taken in another beaker C. 0.25 mL of 3-aminopropysilane was taken in 3 ml of the syringe. The methanol and TMOS were received from Sigma Aldrich and 3-aminopropysilane from ACROS organics. After that, all the mixture of A, B, C, and 3-aminopropysilane were mixed and stirred for 45 seconds. The La_2O_2S: Eu phosphor was then put in a dot pattern in the bottom of the mold. After that mixture was poured into molds. For the top pattern, La_2O_2S: Eu powder was then put on the surface of mixture in the space not directly above the dot pattern of the bottom. When the gel was formed, the methanol was poured over the surface to prevent cracking and the molds were covered by parafilm to prevent contamination and were allowed to stand for 3 hours. All these synthesis processes were performed inside a fume hood. After 3 hours, the gel was transformed from molds to a jar containing a methanol solution and was put for 24 hours. The

methanol solution was then replaced by acetonitrile solution and was waited for 24 hours. The acetonitrile was received from Fisher chemicals. The process of changing acetonitrile was performed 4 times. Finally, to remove the solvents from the pores of aerogel, it was then dried in a critical point dryer CPD model E3100-060. The acetone/ acetonitrile was replaced by CO_2 during the number of flushes with CO_2 at 18 ^{0}C. Usually, in five flushes all the acetone and acetonitrile was completely removed. Then the temperature was set to 40 ^{0}C and after 30 minutes the supercritical point was reached with 1250 psi pressure and at 38 ^{0}C temperature. Once the supercritical point was reached, the supply of CO_2 was turned off and slowly released the CO_2 inside the dryer. When the gas released completely the aluminum boat was taken out and the dried sample was ready. Finally, samples were tested using 3-M tape to ensure good adhesion between the powder and the substrate and no phosphor particles were detached from the base. Enough powder was used to make each spot opaque. Two different thicknesses d= 2.2 mm and 6.3 mm silica aerogel sample were prepared. Every attempt was made to create aerogel thicknesses close to those of Sylgard184. However, experimental challenges lead to unintended thickness variations. Thickness reported here are actual values, not target values.

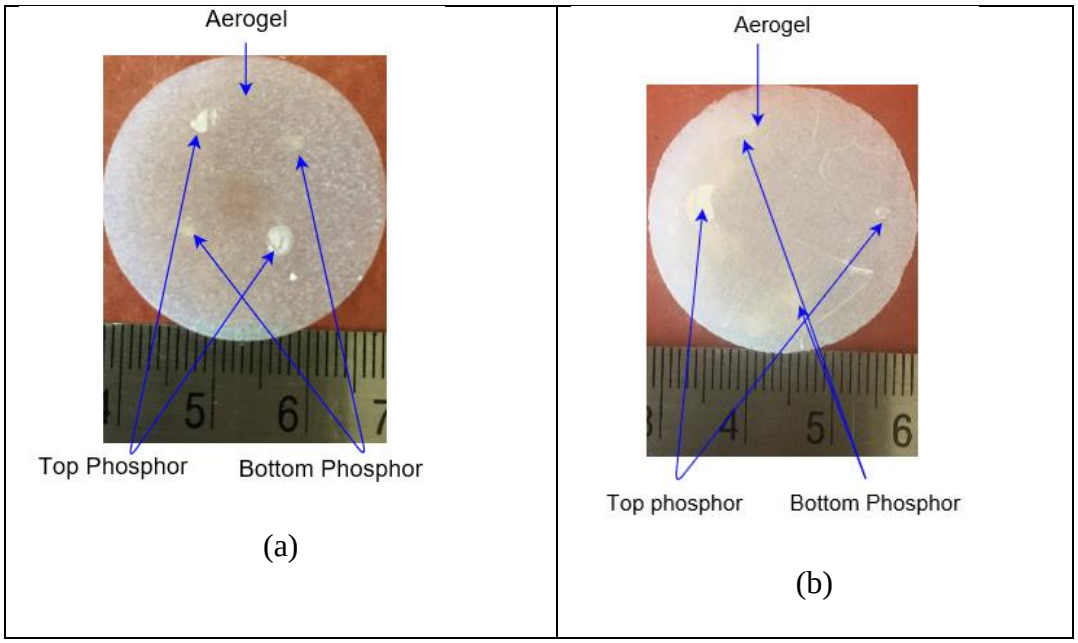

Figure 3.5: Silica aerogel sample with La_2O_2S: Eu phosphor having a thickness (a) 2.2 mm and (b) 6.5 mm

3.1.4 Silica aerogel-$Mg_3F_2GeO_4$: Mn phosphor composite synthesis

The silica aerogel samples with $Mg_3F_2GeO_4$: Mn phosphor was made by the same process as 3.1.3 but used $Mg_3F_2GeO_4$: Mn phosphor instead of La_2O_2S: Eu. In the preparation of silica aerogel samples for both types of phosphor, samples were tested using 3-M tape to ensure good adhesion between the powder and the substrate and no phosphor particles were detached from the base. Enough powder was used to make that spot opaque.

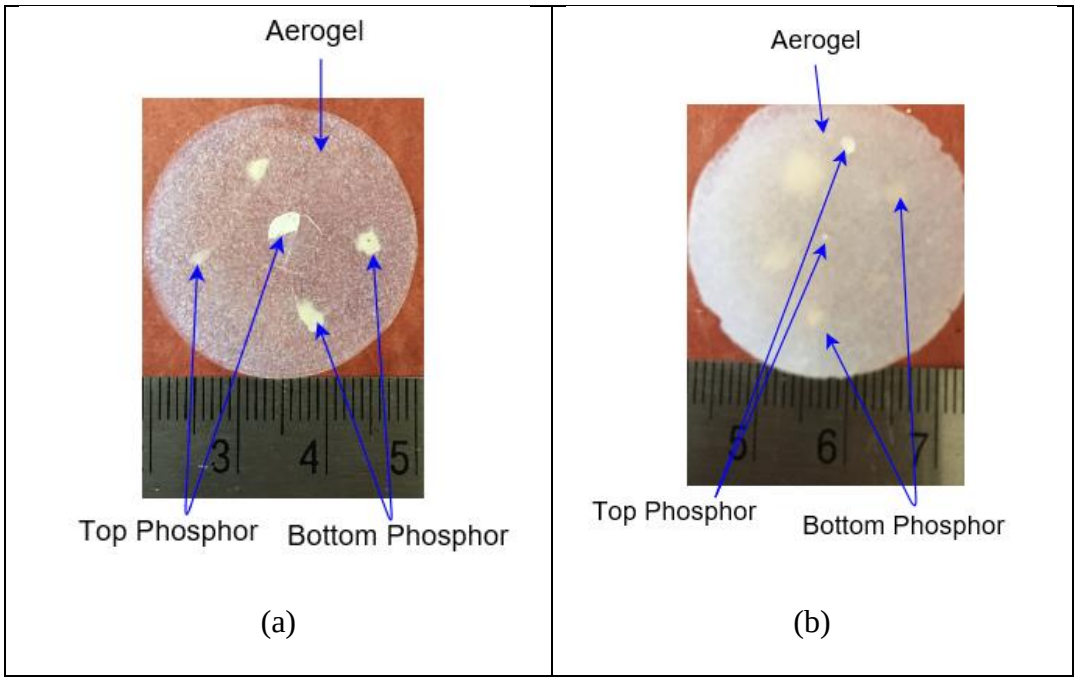

Figure 3.6: Silica aerogel-$Mg_3F_2GeO_4$: Mn phosphor composite with thicknesses (a) 2.2 mm and (b) 6.3 mm

3.1.5 Sylgard184-upconverting phosphor composite synthesis

In this case, Sylgard184 upconverting phosphor composites were made. The phosphor used were lanthanum oxysulphide doped with ytterbium, erbium (La_2O_2S: Yb, Er) and yttrium oxysulphide doped with ytterbium, erbium (Y_2O_2S: Er, Yb).

Sylgard184 silicone elastomer base and curing agent were weighed in Fisher XE series 100A microbalance and were mixed in the ratio of 10:1. The 15 % by weight of Y_2O_2S: Er, Yb phosphor powder was weighted in the same microbalance and added to the mixture. The mixture was then stirred thoroughly and was outgassed in a Precision model 19 vacuum oven until all air bubbles were removed. At the end of the process, it was cured in Cascade Tek vacuum oven at 80 ^{0}C for 1 hour. In this way, Sylgard184 with 15% of Y_2O_2S: Er, Yb samples were prepared.

In a similar manner by putting La_2O_2S: Yb, Er in place of Y_2O_2S: Er, Yb and following the same procedure, Sylgard184 with 15 % of La_2O_2S: Yb, Er samples were obtained. In both cases, the thickness of the sample was 1 mm.

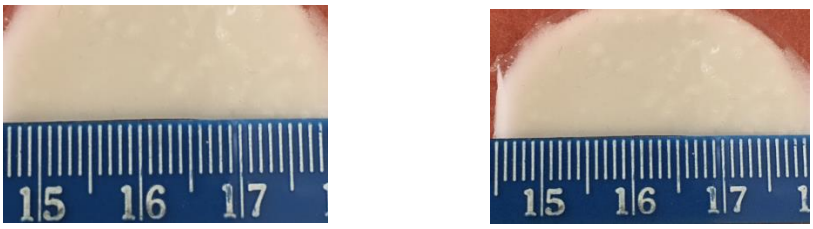

(a) (b)

Figure 3.7: Sylgard184 with 15 % of (a) $Y_2O_2S:Er^{3+}$ Yb^{3+} phosphor composite (b) La_2O_2S: $Er^{3+}Yb^{3+}$ phosphor composite

3.1.6 Imaging and microscopy

Scanning electron microscopy (SEM) was used to image the phosphor powders prior to adding them to the polymer matrix. The phosphors while in powder forms were coated with 20 nm layer of Au/Pd and imaged with a Phenom SEM.

The surface roughness of the samples was also of interest and surface roughness was investigated by means of a Profilm 3D profilometer from Filmetrics. The objective lens used to scan the surface was a Nikon 10X lens. Several different locations were imaged from each samples type.

3.2 Sample for the high temperature ceramic experiment

3.2.1 Ceramic samples

Flexible ceramic ribbons were acquired from from ENrG Inc. This ultra-thin flexible Zirconia Ribbon Ceramic was prepared by R2R method and had a 40 µm thickness. Experiments performed are described below.

3.2.2 Heat distribution assessment

To study the heat distribution and propagation in a ceramic sheet, 2 cm in length and 1.6 cm wide piece of ceramic was taken. Then manganese activated magnesium flurogermanate phosphor ($Mg_3F_2GeO_4$: Mn) was mixed with high temperature glue and coated on the surface of ceramics. The high temperature glue was from VHT Product Company. The maximum temperature the glue can withstand without flame was 1093 ^{0}C. The coated phosphor was dried by leaving for 4 hours at room temperatures. Then this phosphor ceramic composite was placed in the INSTEC HP1200G heating stage equipped with MK 2000 temperature controller. The minimum resolution of this temperature controller is 0.001 ^{0}C. To study the temperature profile, luminescence was taken at four points. Two points were located at the middle of the ceramic and two were located at two edges as shown in Figure 3.8. The luminescence setup consists of light emitting diode (LED) diode and stands tools from Thorlabs. The LED diode of 405 nm for excitation of the phosphor and 650 nm with 40 FWHM band pass filter to detect the luminescence was used. This optical signal is then converted into an electrical signal from photomultiplier tube and sent to the Tektronix 2012 C digital oscilloscope. BNC 575 model pulse generator was used

to excite the phosphorescence. Finally, the decay time was calculated in excel and this decay time was converted to temperature with calibration data. In this way, the temperature profile obtained.

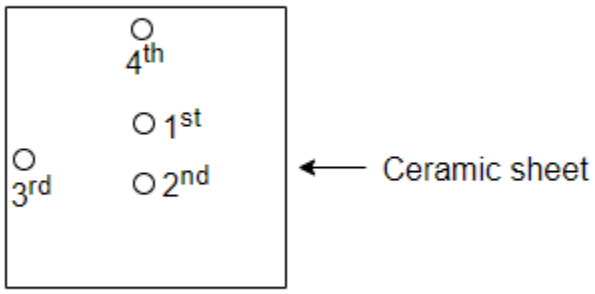

Figure 3.8: Location of points taken on a ceramic sheet

3.2.3 Mechanical testing

The flexural strength of the ceramic sheet was tested performed with mark-10 three point bending apparatus equipped with a force gauge whose capacity was 100 N. The flexural strength was tested at three different temperatures – at liquid nitrogen temperature, room temperature and at 400 ^{0}C. First, the flexural test was performed at room temperature. For liquid nitrogen temperature, the sheet was dipped in liquid nitrogen for 1 hour and immediately transferred to the testing setup. For measurement at 400 ^{0}C, the sheet was heated in the stage and then transferred to the stage and testing was performed. The ceramics sample taken was 7 cm long, 1.6 cm width and 40 µm thick. Two supporting pins were located at 5 cm apart and the loading pin was in the middle of supporting pins.

3.2.4 Thermal barrier behavior of ceramic

In this section of the study, the effect of the ceramic sheets on heat distribution in Sylgard184 and silica aerogels was investigated. For Sylgard184 and aerogel, the chemical and material properties limit the maximum temperature operation. A ceramic piece of 2 cm in length and 1.6 cm wide was taken for this experiment. The same INSTEC heating stage described as before was used in this case also. The Sylgard184 and aerogel was cut into 1 cm in length, 6 mm in breadth and 3 mm in height. The stage temperature was ramped from 25 ^{0}C to 500 ^{0}C at the ramp rate of 20 ^{0}C per minutes. The aerogel was placed in direct contact with the stage. The aerogels were carefully monitored for signs of failure and fatigue and the experiment was aborted before complete failure of the sample being tested. The same procedure was repeated with 1, 2 and 3 layers of ceramic sheet. The experiment was conducted three times and the average was calculated. The procedure was again adopted for Sylgard184.

3.2.5 Sample to study luminescence at high temperature

To study the luminescence at a higher temperature, the Gadolinium oxysulfide doped with europium (Gd_2O_2S: Eu), UKL63/N-X Lot No. 2102, was coated on the surface of a ceramic as mentioned above with the help of high temperature glue. Another phosphor, Dysprosium-doped yttrium aluminum garnet (YAG: Dy) phosphor, QMK66E/N-X, Lot No. 25109, was also used and studied. Both phosphors were acquired from Phosphor Technology UK. The coated phosphor was dried by leaving for 4 hours at room temperatures and finally measurements was performed.

3.3 Sample characterization and testing

3.3.1 Porosimetry measurement of silica aerogel

The NOVAtouch LX2 pore size and surface area analyzer from quantachrome instruments were used to study the surface area, pore size and pore diameter of silica aerogel. A small piece of silica aerogel having mass 0.016 gm whose density was 0.21 gm/cm^3 was taken. Then the sample was inserted into a cylindrical glass vessel and put into a hot bath at 100 ^{0}C for 3 hours. This hot bath removes the water vapors and another dust particle in the aerogel. After that, the tube was transferred to the measurement unit. Liquid nitrogen was used to take the standard measurements at cryogenic temperature. This instrument gives the pore size information based on gas adsorption or desorption. The instruments were connected to the computer with Quantachrome TouchWin^{TM} software. The instruments took 6 hours to collect data. Finally, all the information was available in the computer software.

3.3.2 Thermal conductivity measurement of silica aerogel

Two identical silica aerogels having 3.9 cm in diameter and 0.65 cm in thickness was used to measure the thermal conductivity. The Kapton sensor having radius 3.189 mm was inserted between the two samples. The measurement was performed in Hot Disk TPS 1500 thermal constants analyzer from Thermtest Inc.

3.4 Temperature dependent luminescence setup

A MK 1000 Instec heating-cooling stage equipped with a liquid nitrogen pump and the reservoir was placed inside an ETS environmental chamber that was attached to a dehumidification

system. The dehumidification system controls the humidity inside the chamber. The luminescence was studied at a cryogenic temperature as well as higher temperature. For cryogenic temperature, the continuous supply of liquid nitrogen was required to maintain the low temperature. Once the sample was sufficiently cooled after reaching the required temperature, the decay curve was saved for analysis. To get the information of humidity a sensor was inserted inside the environmental chamber and was connected to the humidifier controller. The environmental chamber was then sealed off from the atmosphere and the pump down process began. After 15 minutes a humidity level of 2.0 % was reached and maintained throughout the duration of the testing. The MK 1000 controller precisely controls temperature to 0.001°C / 1 mK. After each temperature change, adequate time was allowed between measurements for the system to reach thermal equilibrium. The setup consists of the light emitting diode (LED) and stands tools from Thorlabs. LED diode of 405 nm was used for both the La_2S_2O: Eu phosphor and for $Mg_3F_2GeO_4$: Mn phosphor. The excitation light from LED was incident to the sample at an angle of nearly 45^0. The detector was sitting at a height of 5 cm from the top sample surface. The red with 650 nm with 40 FWHM bandpass filter was used to detect 638 nm emission peak of $Mg_3F_2GeO_4$: Mn phosphor. To detect the 510 nm emission line from La_2O_2S: Eu, 510 nm with 10 nm bandwidth filter was used. The filter used was from Andover corporation. This optical signal is then converted into an electrical signal from photomultiplier tube and send to the Tektronix 2012 C digital oscilloscope. BNC 575 model pulse generator was used to excite the phosphorescence. Finally, the decay time was calculated in Excel.

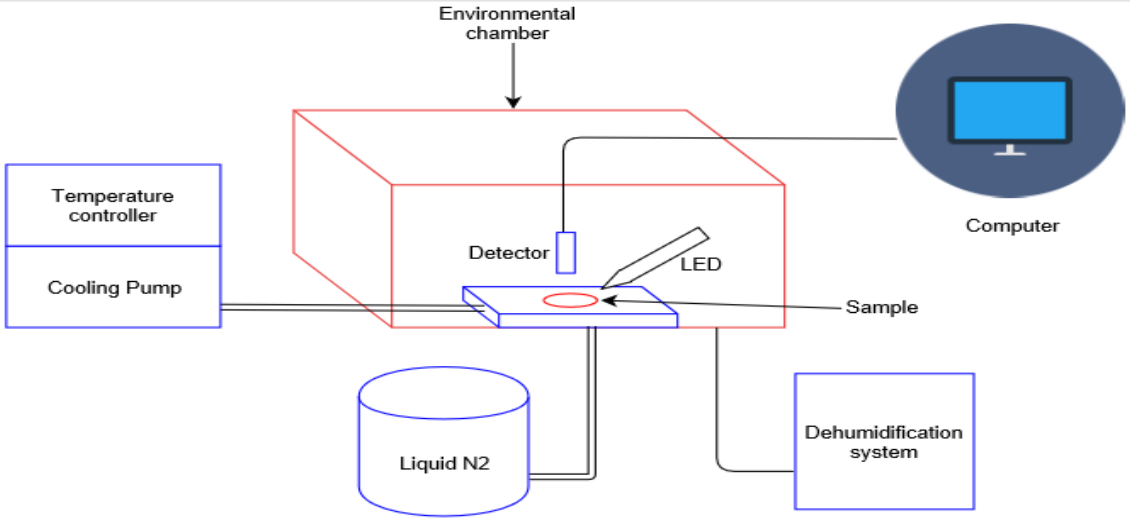

(a)

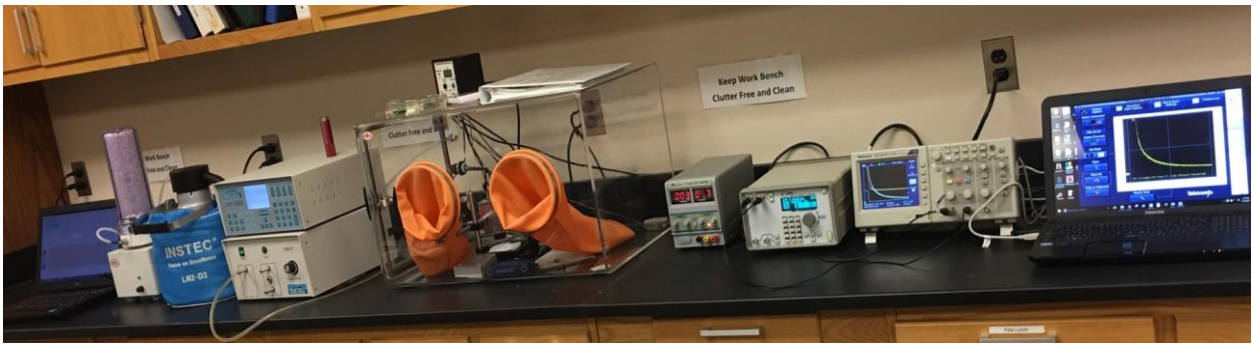

(b)

Figure 3.9: (a) Schematic diagram of test setup and (b) actual setup of the experiment

It was not hard to excite and detect the top phosphor because the detector was just above of it and there was nothing to obstruct the emitted signal. But for bottom side phosphor, careful attention should be given. To know the temperature of the sample which is in contact with the heating/cooling stage, phosphor needs to be excited by UV light and the emitted signal should be detected to find decay time. Sylgard184 and silica aerogel were chosen for this study because these materials are transparent in the visible and UV region. Since the top phosphor was in in off-axis

position then the bottom surface, this enables the detector to capture the emitted signal from bottom side easily. Also, the top and bottom phosphor were created with adequate spacing between them to present any excitation/emission overlap.

3.5 Decay time calculation

The decay time was calculated from the decay curve at various temperature and at different thickness. The file obtained from Tektronix oscilloscope was excel file. The first column was the time in second and the second column was the signal intensity in terms of voltage. This file gave us 2500 data points. Although it was tried to avoid the presence of white light by blocking windows and by covering the environmental chamber with aluminum foil from outside still there was the presence of some white light as background in the signal. To remove this background, the average of first 250 data point was taken and subtracted the average from signal intensity. Then the semi-log of signal voltage along the y-axis and time along the x-axis was plotted and the slope was calculated. Then the reciprocal of this slope gave decay time. The following chart summarizes the temperature finding from decay time.

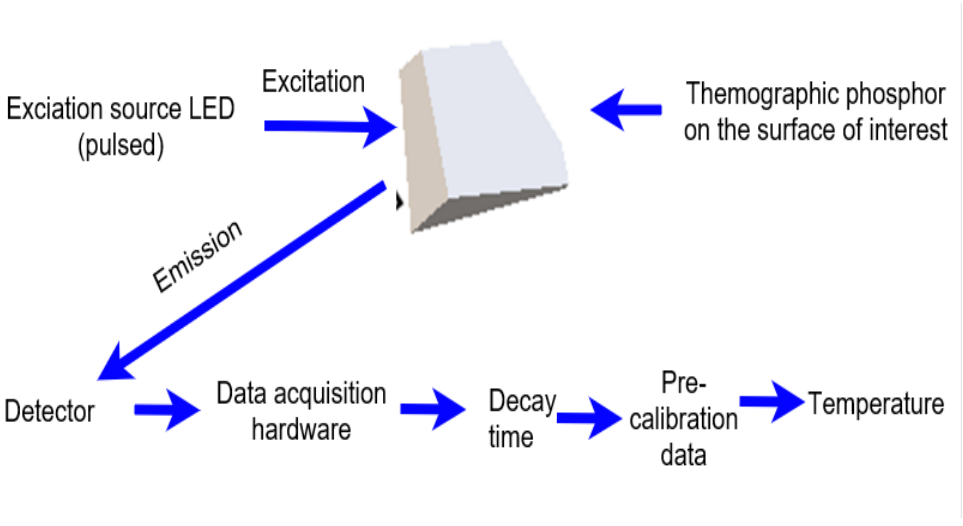

Figure 3.10: Flowchart diagram of temperature calculation

Chapter 4

Results

4.1 Characterization of silica aerogel

4.1.1 Pore size and surface area analysis of native silica aerogel

Silica aerogels synthesized per the method described in Chapter 3 were fully characterized and results are presented here. As previously mentioned the pore size distribution and surface area of the aerogels was evaluated by means of a porosimeter. The single point BET, multipoint BET, and BJH methods were used to investigate the surface area. Pore volume and pore size were obtained through the BJH method. The adsorption and desorption isotherm is shown in Figure 4.1.

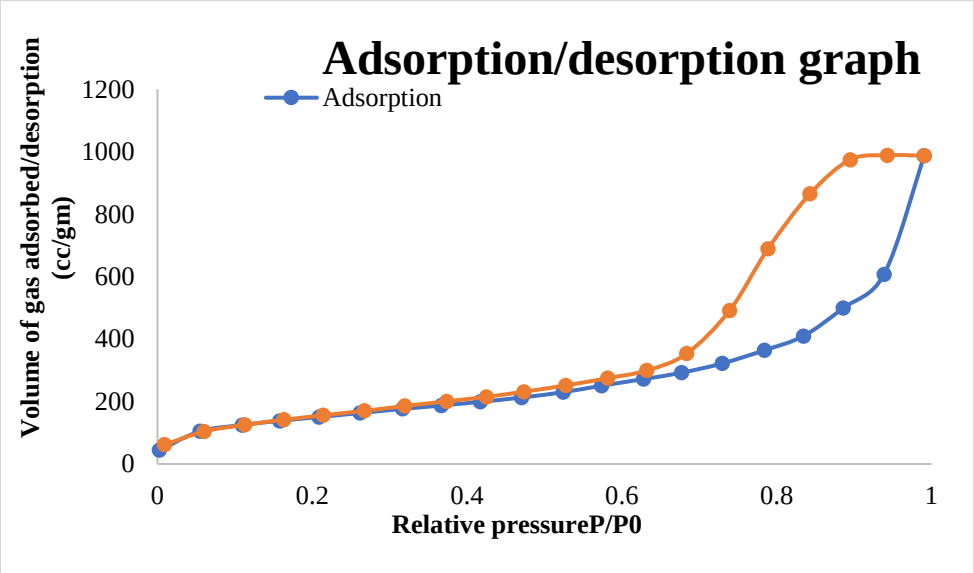

Figure 4.1: The adsorption and desorption isotherm of silica aerogel synthesized for this study

Figure.4.1 shows the pore diameter distribution of the silica aerogels prepared for this study per synthesis method described in detail in Chapter 3. The result shows that the majority of the pores of the silica aerogels prepared here has a diameter between 30 Å to 200 Å. The average pore diameter of this aerogel was found to be 112.7 Å which is in agreement with previously reported values [42].

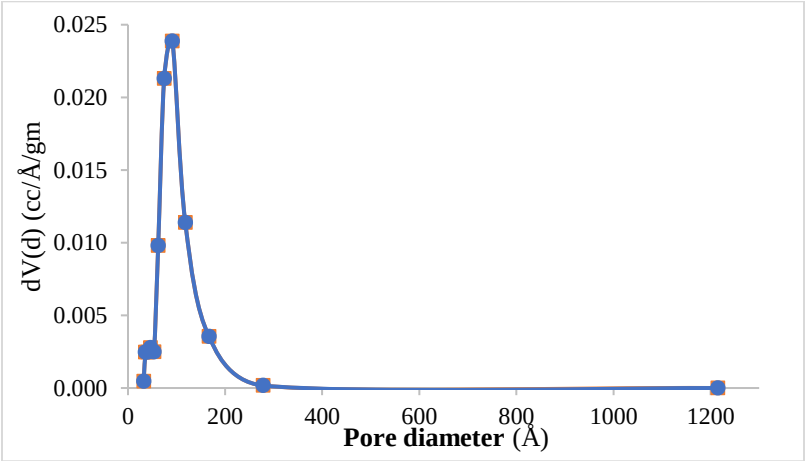

Figure 4.2: Pore diameter distribution of silica aerogel in BJH desorption model

The values of the surface area, pore diameter, and pore volume are presented in table 4.1

Table 4.1: Values of (a) surface areas, (b) pore diameter and (c) pore volume of silica aerogel at different models

	Single point BET	Multipoint BET	BJH adsorption	BJH desorption
Surface area (m^2/gm)	516.0	544.0	374.0	674.9

(a)

	BJH adsorption	BJH desorption	Average pore diameter
Pore diameter (Å)	45.8	91.4	112.7

(b)

	BJH adsorption	BJH desorption	Average pore volume
Pore volume (cc/gm)	1.4	1.6	1.5

(c)

The different surface area was found based on the different model. The BJH desorption model gave the larger surface area which was 674.9 m^2/gm. Similarly, a larger pore volume was obtained in the BJH desorption model which is 1.6 cc/gm.

4.1.2 Thermal conductivity

The thermal conductivity of silica aerogels prepared in this study were measured as described in the previous chapter using a Thermtest unit. Measurements were repeated three times and the average value was 0.064 W/mK. This value is in close agreement with the previously calculated values in the laboratory for aerogels of similar formulations.

4.2 Temperature dependent luminescence of composites

4.2.1 Calibration of La_2O_2S: Eu and $Mg_3F_2GeO_4$: Mn decay behavior

La_2O_2S: Eu and $Mg_3F_2GeO_4$: Mn phosphors in powder form were calibrated and decay behavior is presented in Figure 4.3. For La_2O_2S: Eu phosphor, the temperature dependent 510 nm emission band was calibrated from 15 ^{0}C to -45 ^{0}C. For $Mg_3F_2GeO_4$: Mn, the emission band at 638 nm was calibrated from -100 ^{0}C to 200 ^{0}C for this study.

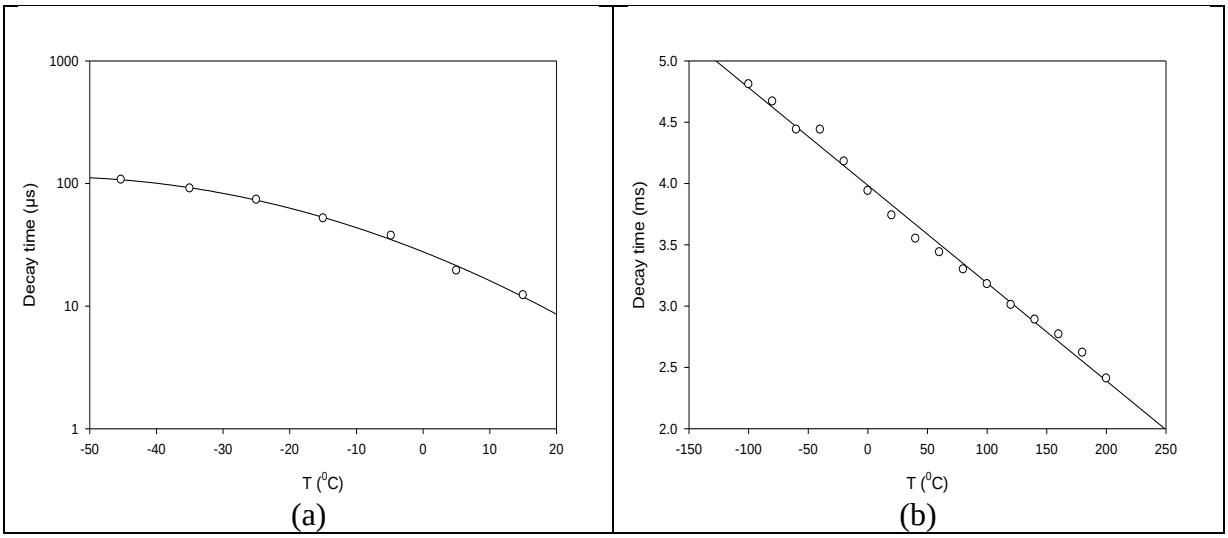

Figure 4.3: Calibration of (a) La_2O_2S: Eu and (b) $Mg_3F_2GeO_4$: Mn phosphors over the temperature range of interest

4.2.2 Temperature dependent luminescence of Sylgard184-La_2O_2S: Eu composites

The luminescence decay characteristics of Sylgard184 samples of different thicknesses with a patterned array of the La_2O_2S: Eu phosphors on both sides was evaluated and results are presented here. Sample thicknesses were d= 3.7 mm, 8 mm and 12 mm and a similar array of phosphor dots was created on both sides, for all samples. In this case, the decay time from the top patch as well as a bottom patch for all thicknesses was calculated. Here, the bottom patch refers to the surface of the sample which is in direct contact with the Instec heating/cooling stage and the top surface refers to the opposite side of the material, separated from the bottom by a distance d. Also, the stage temperature represents the temperature of the heating/cooling stage while the calculated temperature refers to the temperature obtained from the decay time analysis of the emitted luminescence from all samples.

The 510 nm emission line of this phosphor is sensitive below room temperature. So, the luminescence decay characteristics was studied from 20 ^{0}C to – 35 ^{0}C and graphs are shown in Figure 4.3.

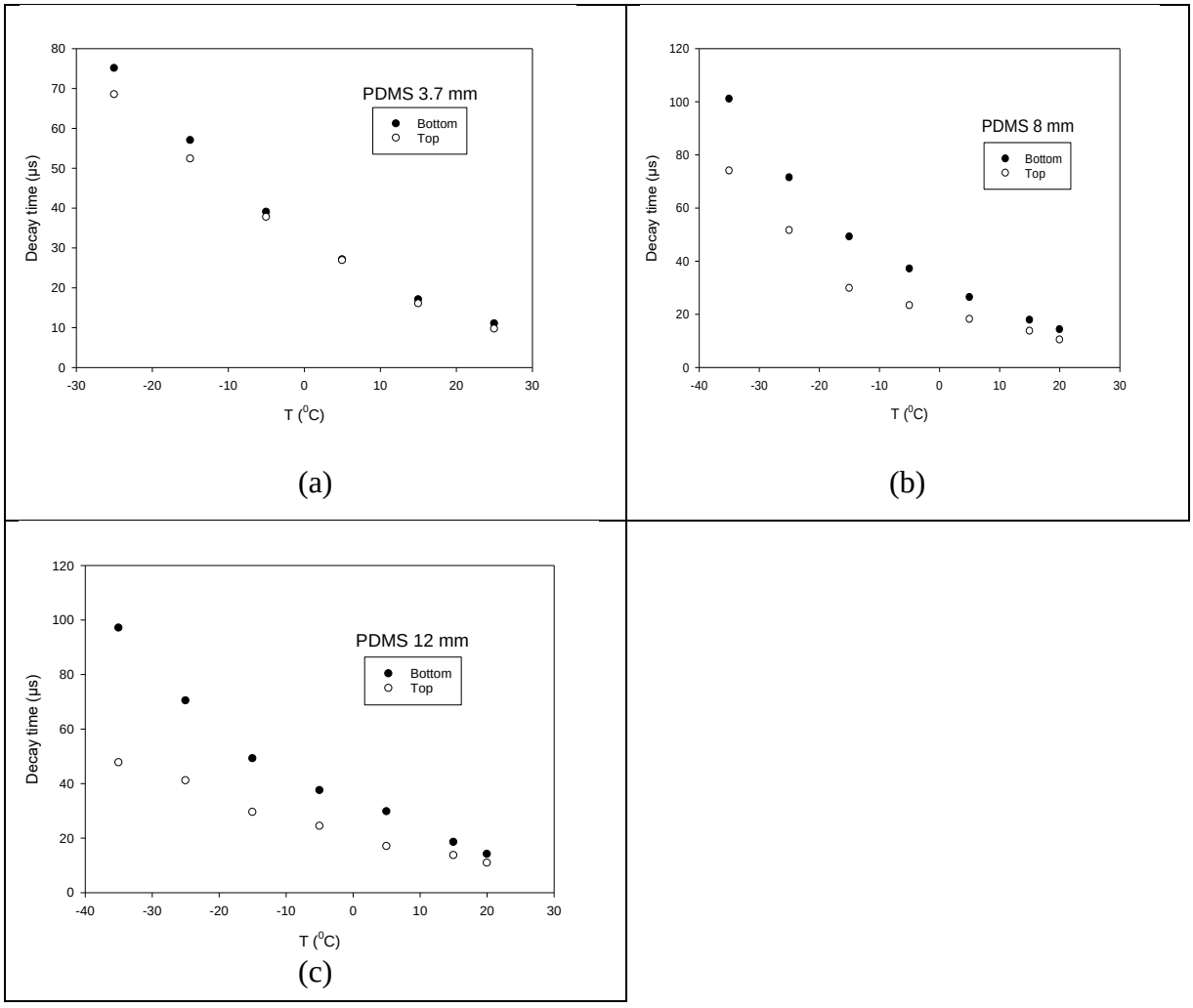

Figure 4.4: Graph of stage temperature vs. decay time of Sylgard184 samples containing La_2O_2S: Eu phosphor patch arrays with thicknesses (a) 3.7 mm, (b) 8 mm, and (c) 12 mm

Figure 4.4 showed that, in decreasing the temperature from 20 ^{0}C, it takes a longer time to decay the emitted signal from both top and a bottom patch of the phosphor. At 20 ^{0}C, the decay time between the top and bottom signal is approximately the same which is expected since both surfaces are at ambient temperature. As the temperature of the stage is lowered by means of the

control software the decay time of the phosphor patch immediately in contact with the stage (bottom) increases which reflect the slower decay that is expected for lower temperatures. The bottom surface is colder than the top surface due to the insulative properties of the material that is sandwiched between the two phosphor patch arrays for the 3.7 mm-thick sample, at a stage temperature of -25 ^{0}C, the difference in the decay time between the top and bottom patches is 6.57 μs. For the 8 mm-thick sample, however, at -25 ^{0}C, the difference in decay time across the material is 19.86 μs. This trend continues as can be seen from data presented in Figures 4 b and 4c where the differences in decay time are affected by the material thickness and the temperature increase.

Using the decay values that were acquired during the experiment and shown in Figure 4.4, the surface temperatures for both top and bottom patches were calculated and presented in Figure 4.5. The decay time obtained in section 4.2.2 is compared with the calibration curve to find the corresponding temperature. The stage temperature was plotted on the horizontal axis and the calculated temperature from decay time appears on the vertical axis. The graphs for all three thicknesses are shown in Figure 4.5.

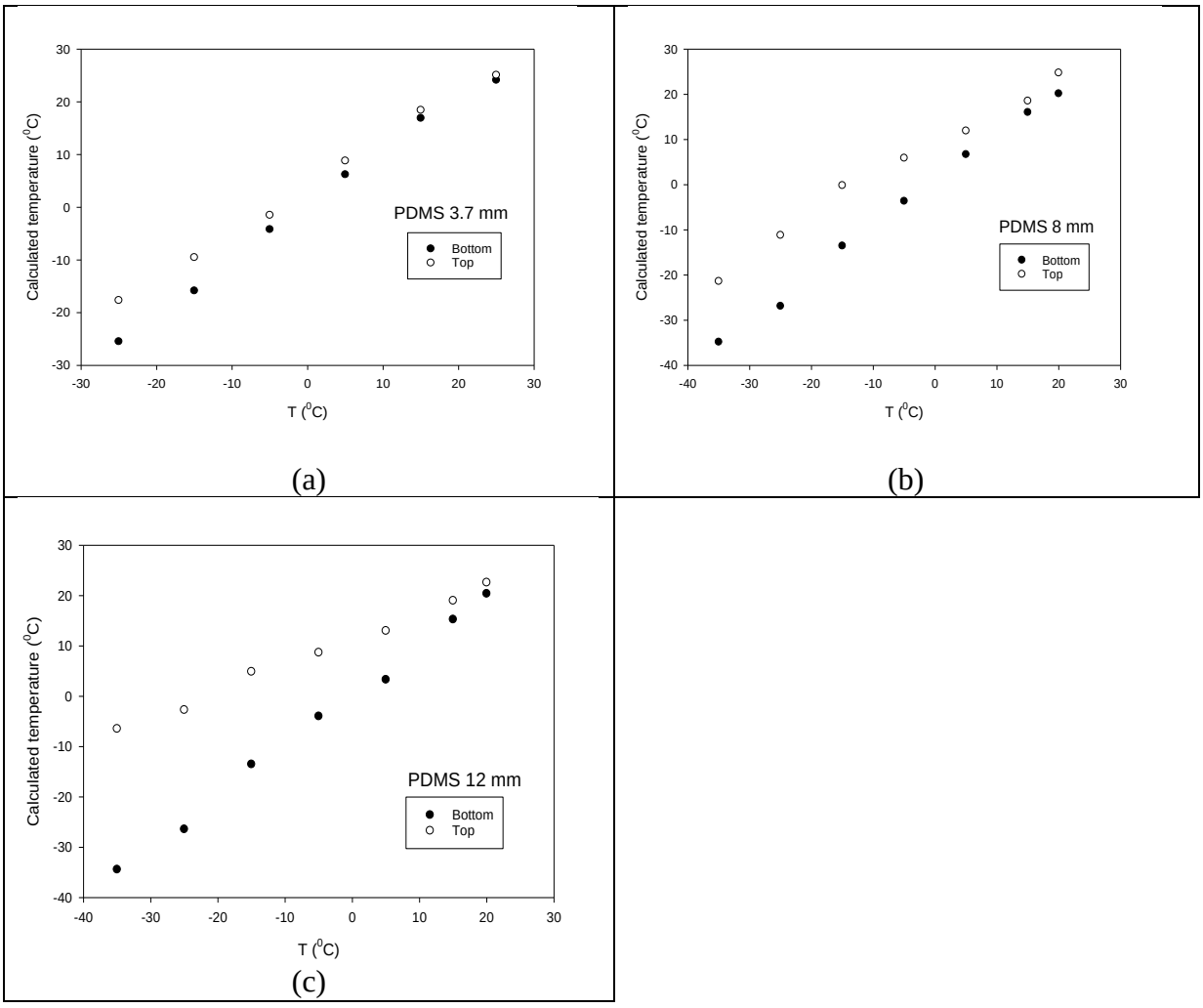

Figure 4.5: Graph of stage temperature vs. calculated temperature of Sylgard184- La_2O_2S: Eu composites for (a) 3.7 mm, (b) 8 mm and (c) 12 mm

From the Figure 4.5, it was noted that the temperature difference near room temperature is minimum. That means the temperature on both surfaces is nearly the same. As the temperature goes down from room temperature, the significant temperature difference was observed. It can be seen from all graphs, there is a temperature gradient across the polymer slab and not surprisingly this gradient increase with increasing sample thickness d.

The temperature difference graph along with the stage temperature is shown in Figure 4.6.

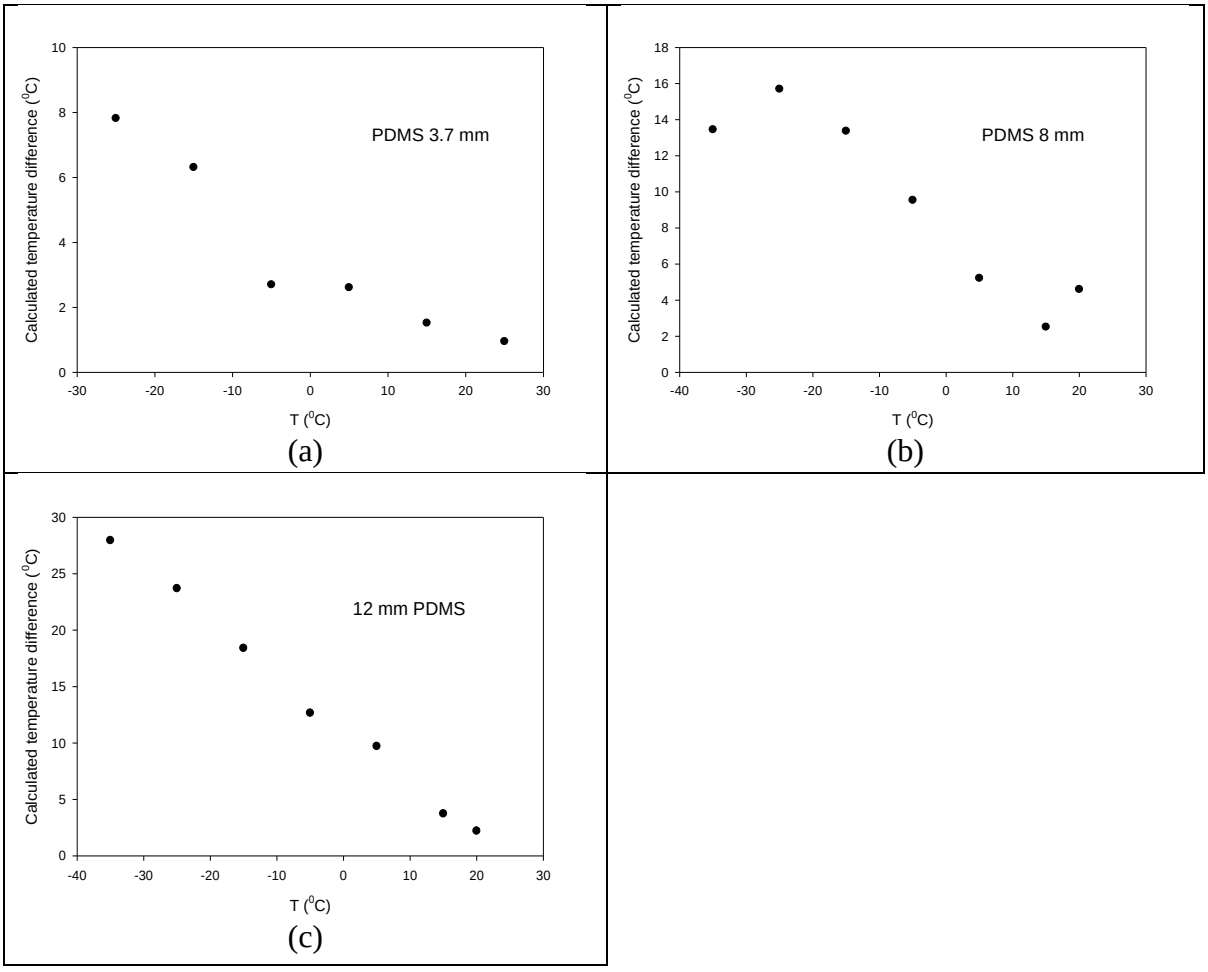

Figure 4.6: Graph of stage temperature vs. calculated temperature difference (ΔT) between the top and the bottom surface of Sylgard184- La_2O_2S: Eu composites for (a) 3.7 mm, (b) 8 mm and (c) 12 mm thick sample

From Figure 4.6, it was discovered that the temperature difference increases linearly with stage temperature. The thicker the sample, less amount of heat transferred to the other surface of the sample. Results confirm that it is possible to interrogate both sides of the Sylgard184-phosphor composite and infer accurate temperature information that can be utilized for calculating heat flux and ultimately designing a flexible heat flux gauge.

4.2.3 Temperature dependent luminescence of Sylgard184-$Mg_3F_2GeO_4$: Mn composites

The $Mg_3F_2GeO_4$: Mn phosphor was also investigated in a manner similar to what was described in section 4.2.2. This phosphor was chosen to complement the range that La_2O_2S: Eu did not cover. The $Mg_3F_2GeO_4$: Mn phosphor has a temperature dependent emission line at 650 nm and is detectable at higher temperatures, up to ~1000ºC. Luminescence behavior of this phosphor from -45 ^{0}C to 200 ^{0}C was studied. The results are shown in Figure 4.7.

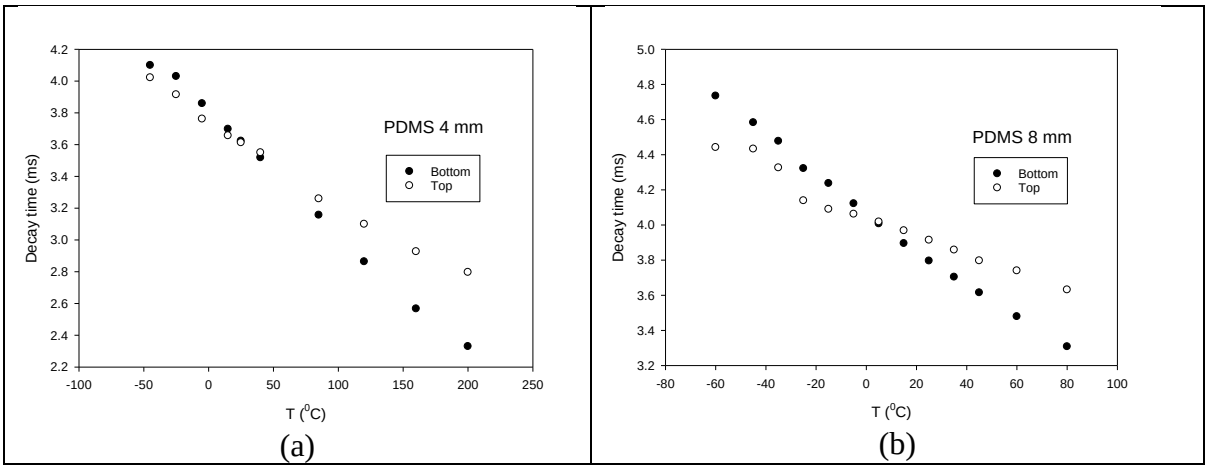

Figure 4.7: Graph of stage temperature vs. decay time of Sylgard184 samples containing $Mg_3F_2GeO_4$: Mn phosphor patch arrays with thicknesses (a) 4 mm and (b) 8 mm

From Figure 4.7, It can be seen that the decay time of both surfaces is almost same at room temperature that is at 25 ^{0}C. It was noticed that, below room temperature, it takes a longer time to decay the bottom patch signal than the top. But, above room temperature, it was observed the opposite. The top patch emission takes a longer time to decay than the bottom patch emission. Since the Sylgard184 has small thermal conductivity only the small amount of heat transferred from the higher surface temperature to lower surface temperature.

Figure 4.8 is the plot of the temperature difference between the top and bottom surfaces of Sylgard184 samples of different thicknesses as a function of the stage temperature.

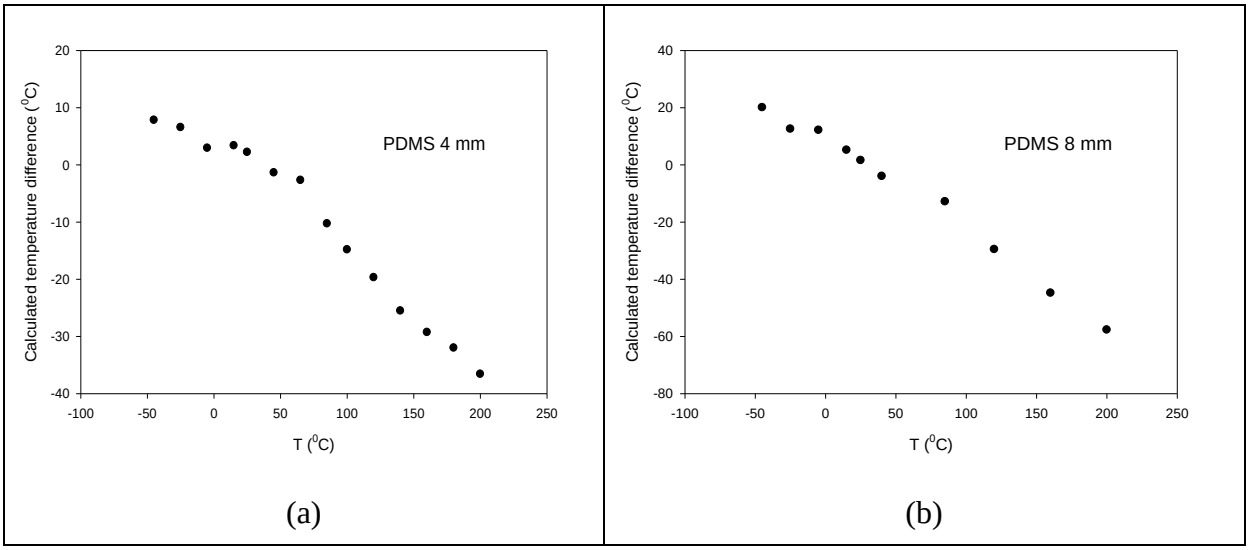

Figure 4.8: Graph of stage temperature vs. calculated temperature difference (ΔT) between the top and a bottom surface of Sylgard184- $Mg_3F_2GeO_4$: Mn composites for (a) 4 mm and (b) 8 mm thick sample

Figure 4.8 shows that higher the thickness higher will be the temperature difference. At -45 ^{0}C, for 4 mm Sylgard184, the difference is 7.82 ^{0}C whereas for 8 mm it is 20.05 ^{0}C.

4.2.4 Temperature dependent luminescence of silica aerogel-La_2O_2S: Eu composites

Aerogel composites containing an array of phosphor patches on both sides of the aerogel were prepared also and the luminescence behavior of these samples was investigated in a manner similar to what was described above for Sylgard184 samples. The time dependent decay characteristics were studied between 15 ^{0}C and -45 ^{0}C and the results of their behavior is shown in Figure 4.9 for two different aerogel thicknesses d=2.2 mm and d=6.5 mm. Using the setup described in Chapter 3, the phosphor patches in direct contact with the stage were excited and their

emission clearly detectable. A key point to note here is that the excitation and emission signals travelling through the aerogel width were detectable with the setup previously described and had a signal to noise ratio that was acceptable. Aerogel samples thicker than 6.5 mm were not prepared for this study due to limitations associated with the critical point dryer and as a result, it was not possible to evaluate the maximum aerogel thickness that this technique could work on.

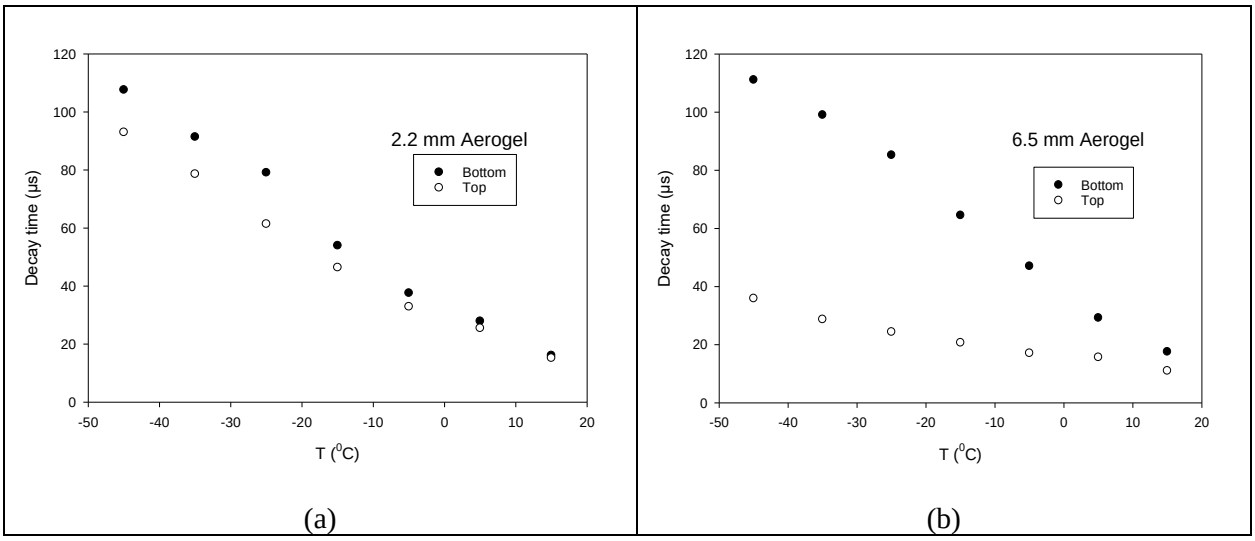

Figure 4.9: Stage temperature vs. decay time of silica aerogel containing La_2O_2S: Eu phosphor patch arrays with thicknesses (a) 2.2 mm and (b) 6.5 mm

Once again, the decay times were used to calculate the temperatures of the phosphor patches on both sides of the material for each stage temperature for both aerogel thicknesses. Results are shown in Figure 4.10. It can be clearly seen that as the aerogel thickness increases the temperature gradient across the material increases also. This is one indicator that the temperature information is being gathered from the intended patch.

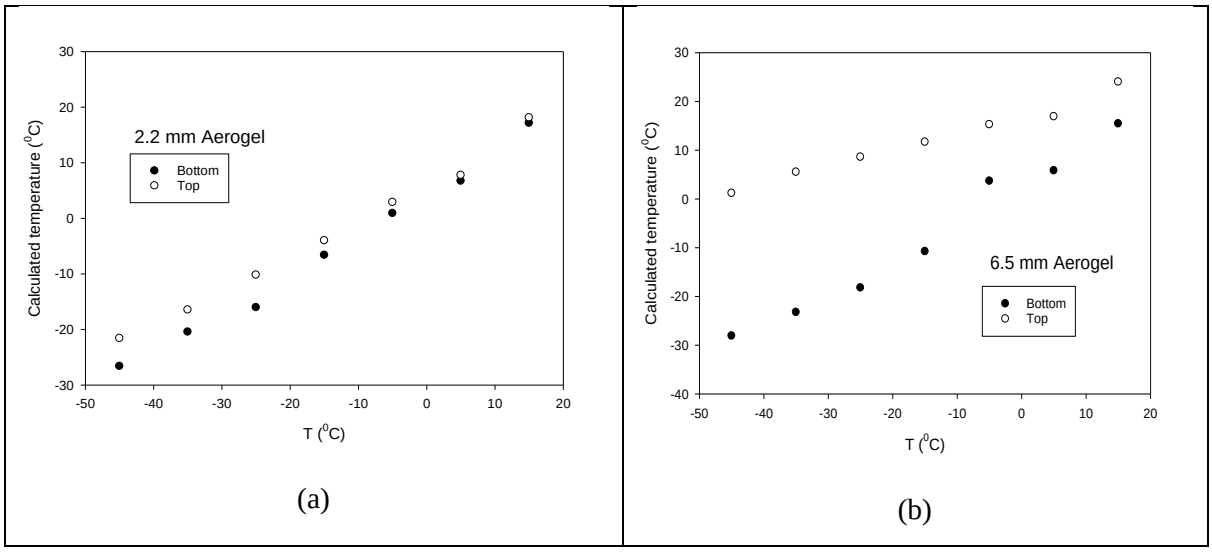

Figure 4.10: Stage temperature vs. calculated temperature of silica aerogel- La_2O_2S: Eu composites for (a) 2.2 mm and (b) 6.5 mm

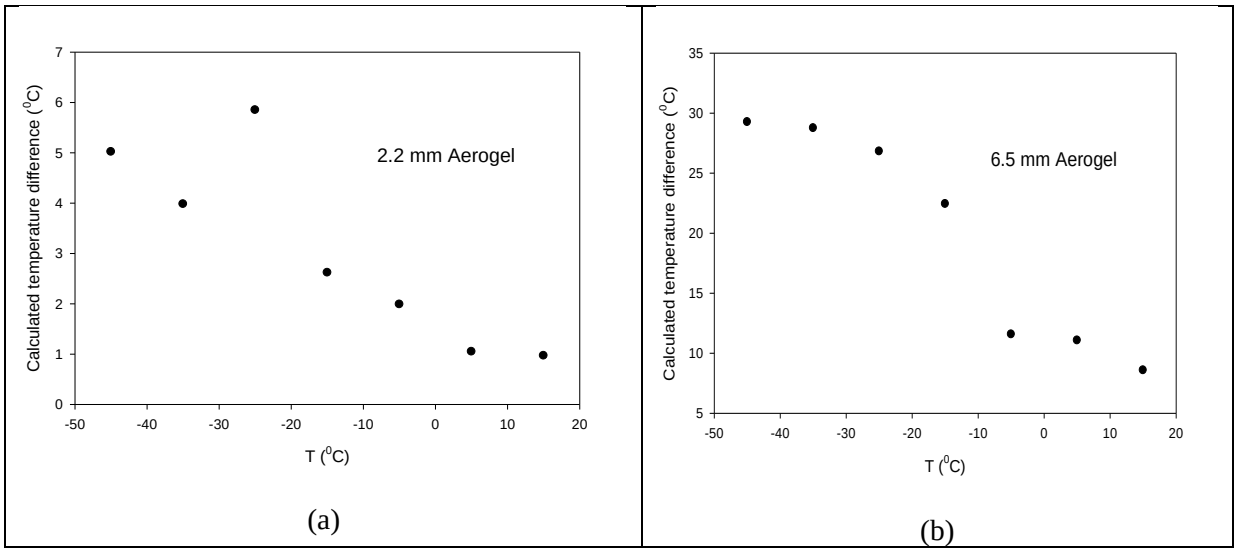

Figure 4.11: Stage temperature vs. calculated temperature difference (ΔT) between the top and the bottom surface of silica aerogel- La_2O_2S: Eu composite for (a) 2.2 mm and (b) 6.5 mm samples

From the graph of decay time vs calculated temperature, it was observed that the time to decay bottom signal is almost equal for both samples. It can be seen that the decay time is linearly dependent upon temperature in the studied temperature region. Figure 4.10 showed that the temperature difference for 6.5 mm aerogel is greater than 2.2 mm for all stage temperatures. For

2.2 mm sample, the temperature difference is only 5.02 ^{0}C at -35 ^{0}C but it is 29.26 ^{0}C for 6.5 mm sample at the same temperature. For the 8 mm Sylgard184, it was only 20.05 ^{0}C at that temperature. These results reflect the lower thermal conductivity of aerogels when compared to Sylgard184 elastomers.

4.2.5 Temperature dependent luminescence of silica aerogel-$Mg_3F_2GeO_4$: Mn composites

The decay characteristics of $Mg_3F_2GeO_4$: Mn phosphor patch on the surface of silica aerogel was studied. The studied samples were d= 2.2 and d=6.5 mm thick. The decay characteristics of $Mg_3F_2GeO_4$: Mn phosphor was investigated as a function of temperature and at every temperature, the emitted signal for the top and bottom patches was recorded. The 2.2 mm thick sample was easily interrogated on both sides of the sample. Exciting the bottom patch and detecting the emitted signal through the material was not hindered by the scatter due to the porous structure of the aerogels. In the case of the 6.5 mm aerogel sample, however, detecting the emitted signal from the bottom patch was challenging and the effects of scattering were clearly interfering with signal detection. This resulted in errors in the inferred decay times and highlighted in Figure 4.12. The intersection of decay line between the top and the bottom surface is expected to occur at approximately room temperature, however, the graph shows that based on signals detected, this intersection occurs below room temperature.

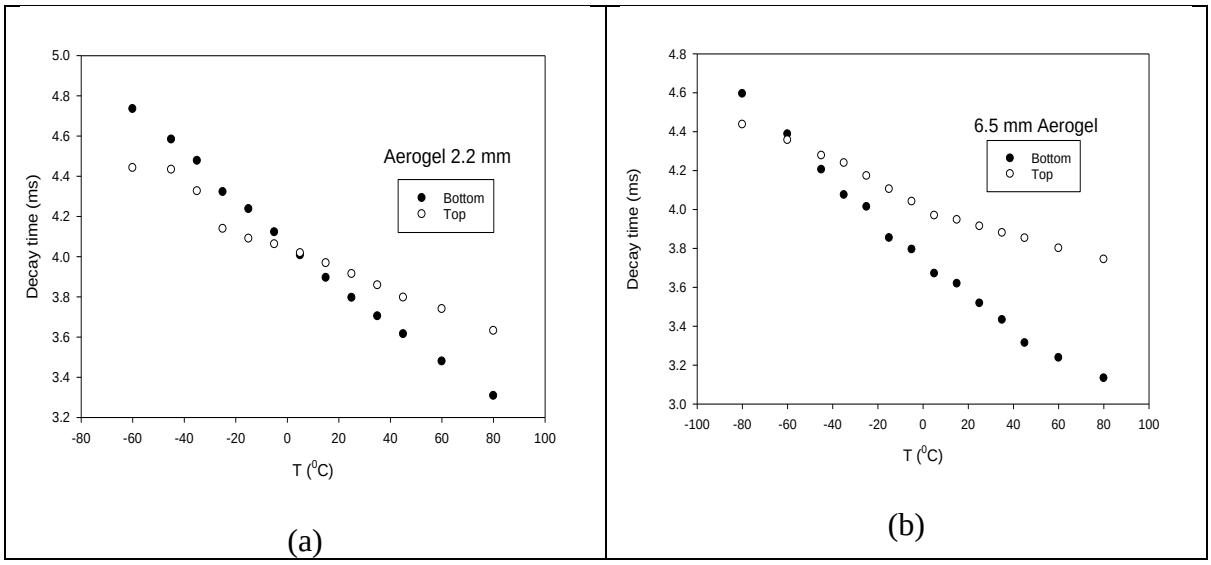

Figure 4.12: Stage temperature vs. decay time of silica aerogel containing $Mg_3F_2GeO_4$: Mn phosphor patch arrays with thicknesses for (a) 2.2 mm and (b) 6.5 mm

The graph of calculated temperature from decay time with stage temperature is also plotted in Figure 4.13 and reflects the differences noticed in the two aerogel samples of different thicknesses.

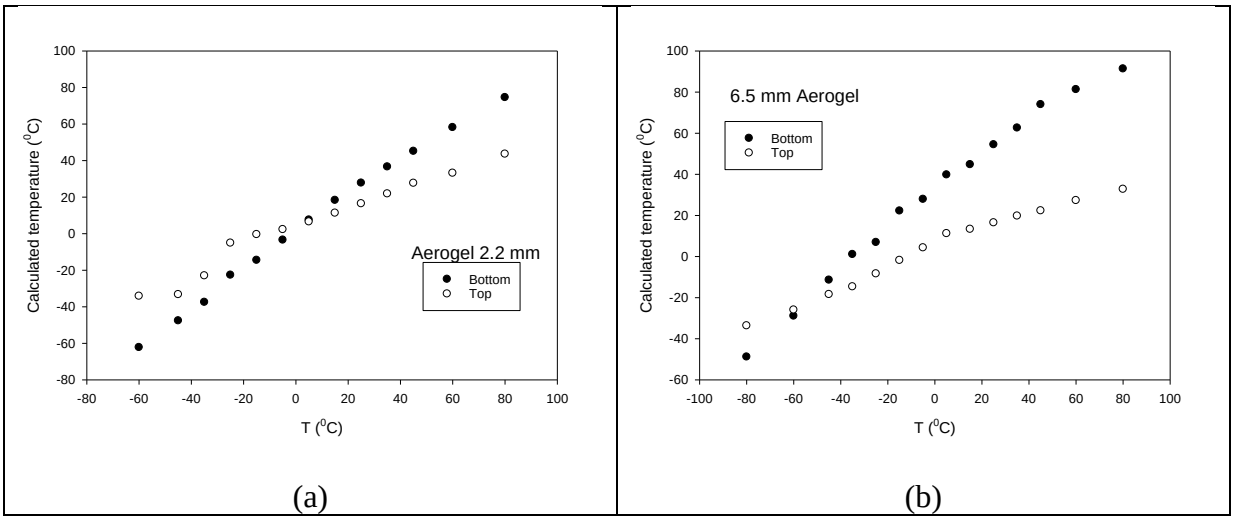

Figure 4.13: Stage temperature vs. calculated temperature of the top and a bottom surface for silica aerogel-$Mg_3F_2GeO_4$: Mn composites for thicknesses (a) 2.2 mm and (b) 6.5 mm

4.2.6 Emission behavior from neighboring phosphor patches

In order to evaluate any statistical variations among the phosphor particles themselves, the luminescence behavior of phosphors from different locations was investigated. A representative data set is shown in Figure 4.14 for an 8 mm thick Sylgard184- $Mg_3F_2GeO_4$: Mn composite. Two points on top and two points on bottom surfaces were taken tested and referred to as 1st and 2nd in the diagram. As can be seen

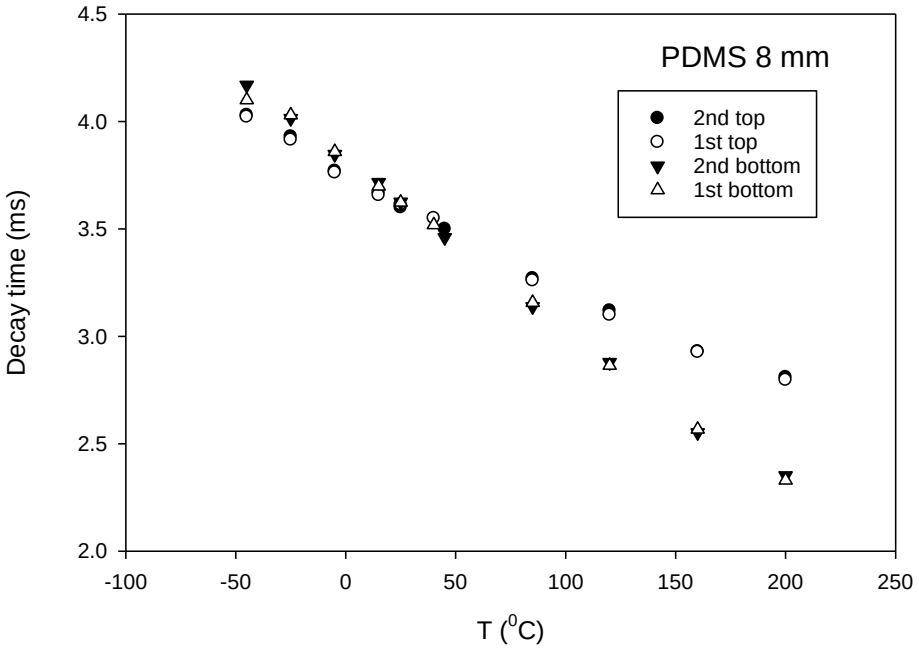

Figure 4.14: Multipoint decay time vs. stage temperature for 8 mm Sylgard184- $Mg_3F_2GeO_4$: Mn composite

the decay time for both points on the top surface as well as on the bottom surface matche very closely. From this data, the consistency of the experiment was noted. Also, it can be said that the phosphor powder is behaving the same at different points on the Sylgard184 surfaces. The same decay time on top surface also indicates the same temperature on both points showing that the heat transfer is the same throughout the samples neglecting the edge effect.

4.3 Heat flux calculation

Heat flux was calculated using Fourier's law in one dimension due to conduction of heat as described in Chapter 2. The heat flux was calculated for 2.2 aerogel-La_2O_2S: Eu phosphor composite and 3.7 mm Sylgard184-La_2O_2S: Eu phosphor composite. In this calculation, the thermal expansion of Sylgard184 was not considered.

Heat flux calculation of 3.7 mm Sylgard-La_2O_2S: Eu and 2.2 mm silica aerogel-La_2O_2S: Eu composites

The calculated heat flux for these samples is shown in table 4.2. The thermal conductivity for Sylgard184 was taken 0.16 W/m.K [43]. For silica aerogel, the value was taken 0.064 W/m.K. The ΔT is the temperature difference between the two surfaces of samples calculated from the decay time. The negative sign shows that the temperature is flowing from higher temperature to lower temperature.

Table 4.2: Heat flux values for 2.2 mm silica aerogel and 3.7 mm Sylgard184 phosphor composites

T (^{0}C)	2.2 mm aerogel			3.7 mm Sylgard184		
	ΔT (^{0}C)	K (W/m.K)	Heat flux (W/m^2)	ΔT (^{0}C)	K (W/m.K)	Heat flux (W/m^2)
-25	5.85	0.064	170.18	7.82	0.16	338.16
-15	2.62	0.064	76.22	6.31	0.16	272.86
-5	1.99	0.064	57.89	2.70	0.16	116.76
5	1.05	0.064	30.55	2.61	0.16	112.86
15	0.97	0.064	28.22	1.52	0.16	65.73

The heat flux for 2.2 mm aerogel and 3.7 mm Sylgard184 was plotted in Figure 4.15.

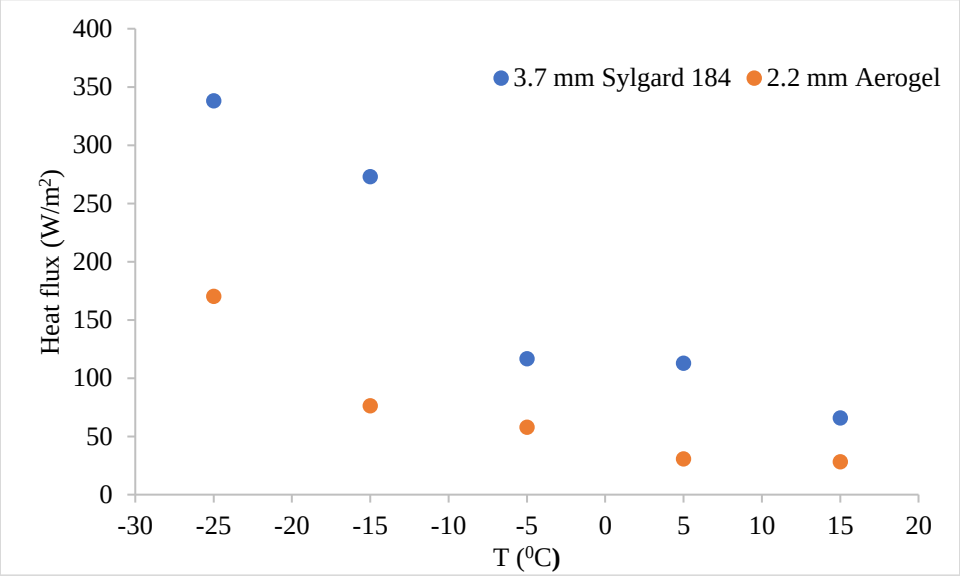

Figure 4.15: Heat flux vs stage temperature for aerogel- La_2O_2S: Eu and Sylgard184- La_2O_2S: Eu composites

Figure 4.15 shows that at 15 ^{0}C, there is minimum heat flux for both sample type. When the temperature is going down the heat flux increases. At room temperature, both surfaces are in thermal equilibrium and there is no transfer of heat. As the temperature of one surface is changed, there will be the temperature difference between two surfaces and heat flows from higher temperature to lower temperature. That is why the heat flux increases as temperature go down from 15 ^{0}C to -25 ^{0}C. It was found that the heat flux is minimum for silica aerogel than Sylgard184 even for a less thick sample. This is because of the low thermal conductivity of silica aerogel. From this, it can be concluded that the silica aerogel is a better thermal insulator than Sylgard184.

4.4 Luminescence of upconverting phosphor

The emission characteristics of these phosphors embedded in Sylgard184 is shown in Figure 4.16. The graph is the fluorescence signal vs time and the normalized signal vs time (insets). The studied temperature was -50 ^{0}C, 25 ^{0}C, 100 ^{0}C and 200 ^{0}C. It was found the change in fluorescence signal level at all temperature as shown in Figure 4.16. For Y_2O_2S: Yb, Er in Sylgard184, the semilog of the signal voltage along with time was plotted to find decay time, but the plot was not straight, so it was difficult to find the decay time for it.

For La_2O_2S: Yb,Er in Sylgard184 the decay time was 0.7, 0.7, 0.6 and 0.45 ms at -50 0C, 25 ^{0}C, 100 ^{0}C and 200 ^{0}C respectively. This shows that the decay time is the same from – 50 ^{0}C to 100 ^{0}C. The decay time was decreased to 0.45 ms at 200 ^{0}C. It may be inferred that this phosphor is sensitive above 200 ^{0}C.

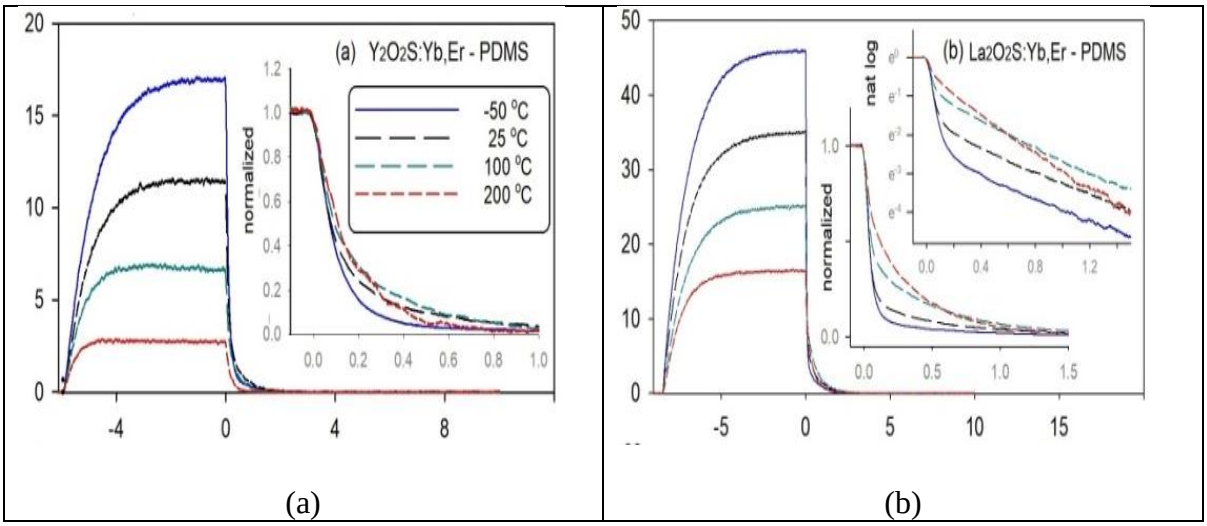

Figure 4.16: Fluorescence signal vs time and normalized signal vs time for decay curve (inset) for (a) Y_2O_2S: Yb, Er in Sylgard184 and (b) La_2O_2S: Yb, Er in Sylgard184

Yang et al. [44] have demonstrated the feasibility of La_2O_2S: Yb, Er phosphor for sensing application by the fluorescence intensity ratio method. Here, in this work, the signal level, decay

time and rise time method was studied for sensing application. The sensors which worked based on the intensity ratio method suffers several problems. For a non-contact application, for the medium which absorbs and scatters light much may alter the spectral ratio and it affects the calibration of sensors, but this effect is not present in case of decay/rise time method.

The normalized rise time graph of both phosphor type embedded in Sylgard184 is shown in Figure 4.17.

From this Figure 4.17, it was observed that the rise time also depends upon the temperature. The sensitivity is different for different temperature range. For La_2O_2S: Yb, Er Sylgard184 sample, the rise time was same from -50 ^{0}C to 100 ^{0}C which was 1.4 ms. The rise time decreased to 1.05 ms at 200 ^{0}C. From this, it may be inferred that the La_2O_2S: Yb, Er doped Sylgard184 shows greater sensitivity above 200 ^{0}C. The rise time was very noticeable between -50 ^{0}C to 200 ^{0}C for Y_2O_2S: Yb, Er Sylgard184 sample. The rise time was found to be 1150 µs, 1050 µs, 650 µs and 440 µs at -50 ^{0}C, 25 ^{0}C, 100 ^{0}C and 200 ^{0}C.

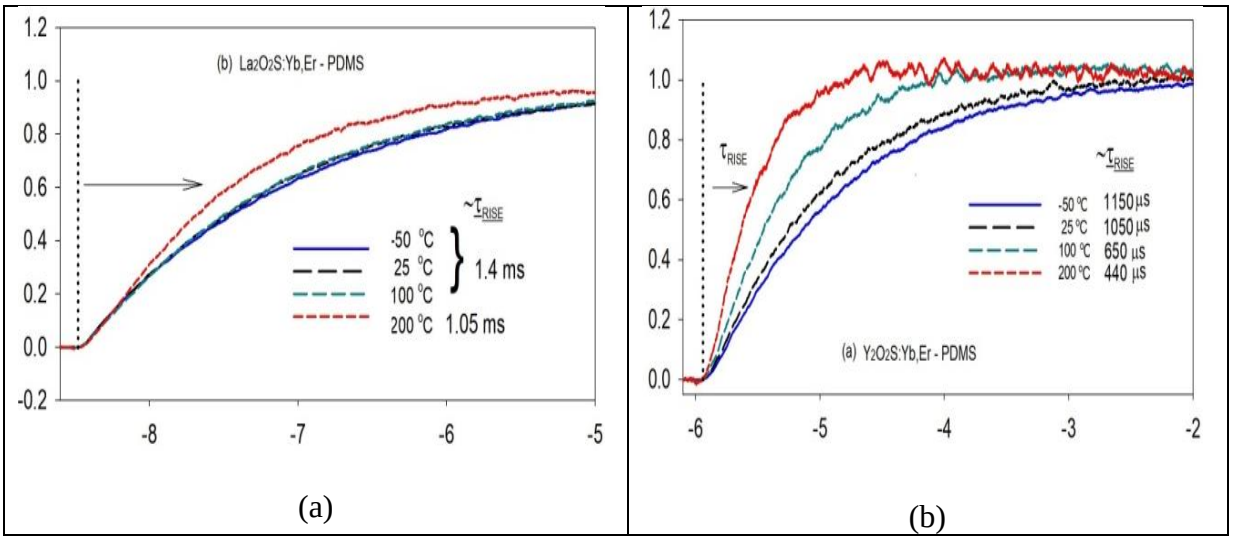

Figure 4.17: normalized fluorescence rises signal vs time for (a) La_2O_2S: Yb, Er in Sylgard184 and (b) Y_2O_2S: Yb, Er in Sylgard184

4.5 Microscopy images

The SEM images of the studied phosphor are shown in Figure 4.18.

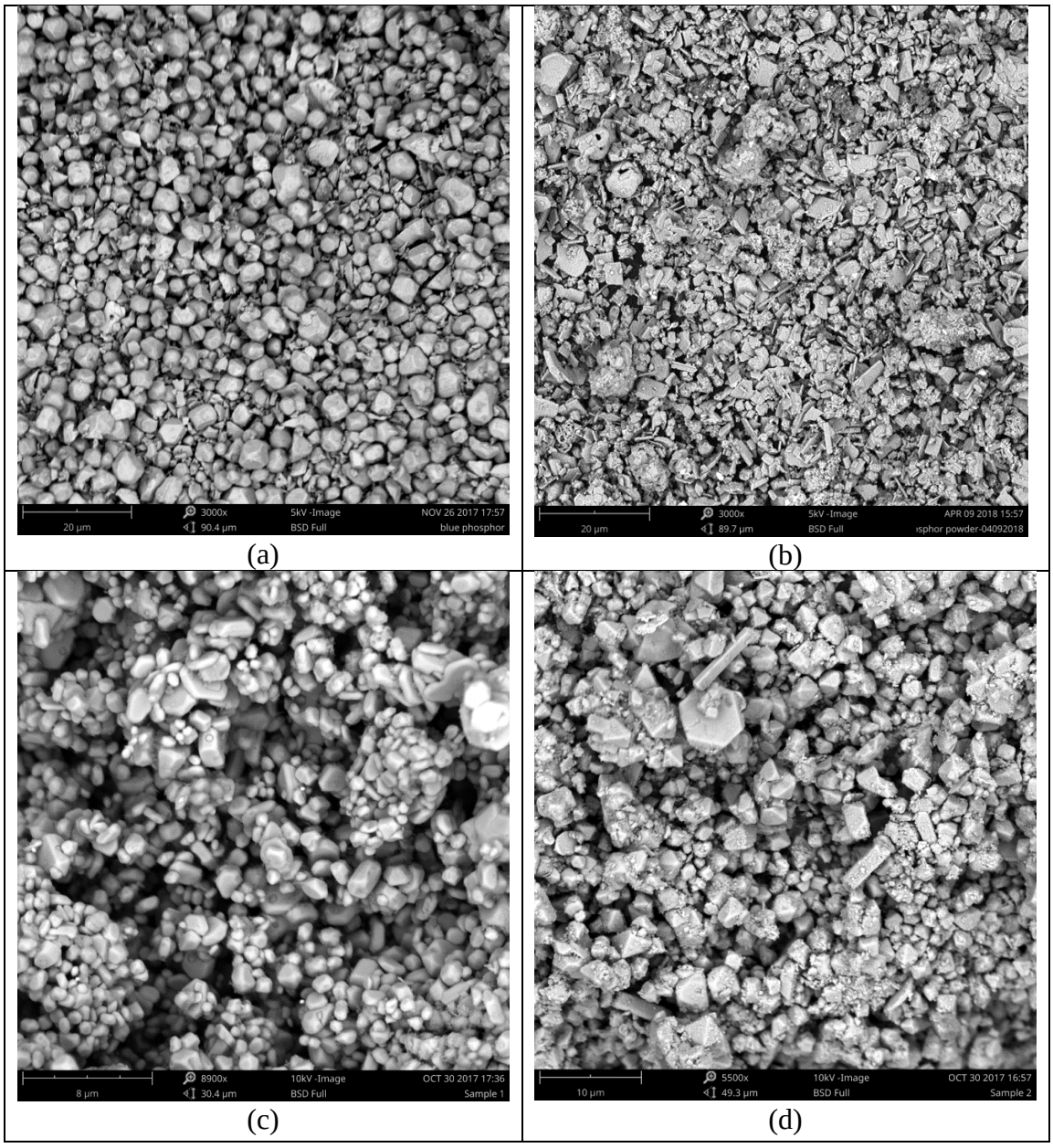

Figure 4.18: SEM images of (a)La_2O_2S: Eu and (b) $Mg_3F_2GeO_4$: Mn (c) Y_2O_2S: Er, Yb and (d) La_2O_2S: Er, Yb

The SEM images showed that there is a noticeable difference in grain size and geometry between the different phosphors. The grain size of the phosphor was found to be a couple of µm.

This observation revealed the microparticle nature of studied phosphor. It was noted that the geometry of Lanthanum host powder with signal doped Figure 4.18 a is different from the double doped powder Figure 4.18 c. It seems that there is an electrostatic charge present in the case of Y_2O_2S: Er, Yb phosphor particle indicating the cluster formation.

The surface roughness images of Sylgard184 and aerogel was obtained. The images are shown in Figure 4.19 and 4.20.

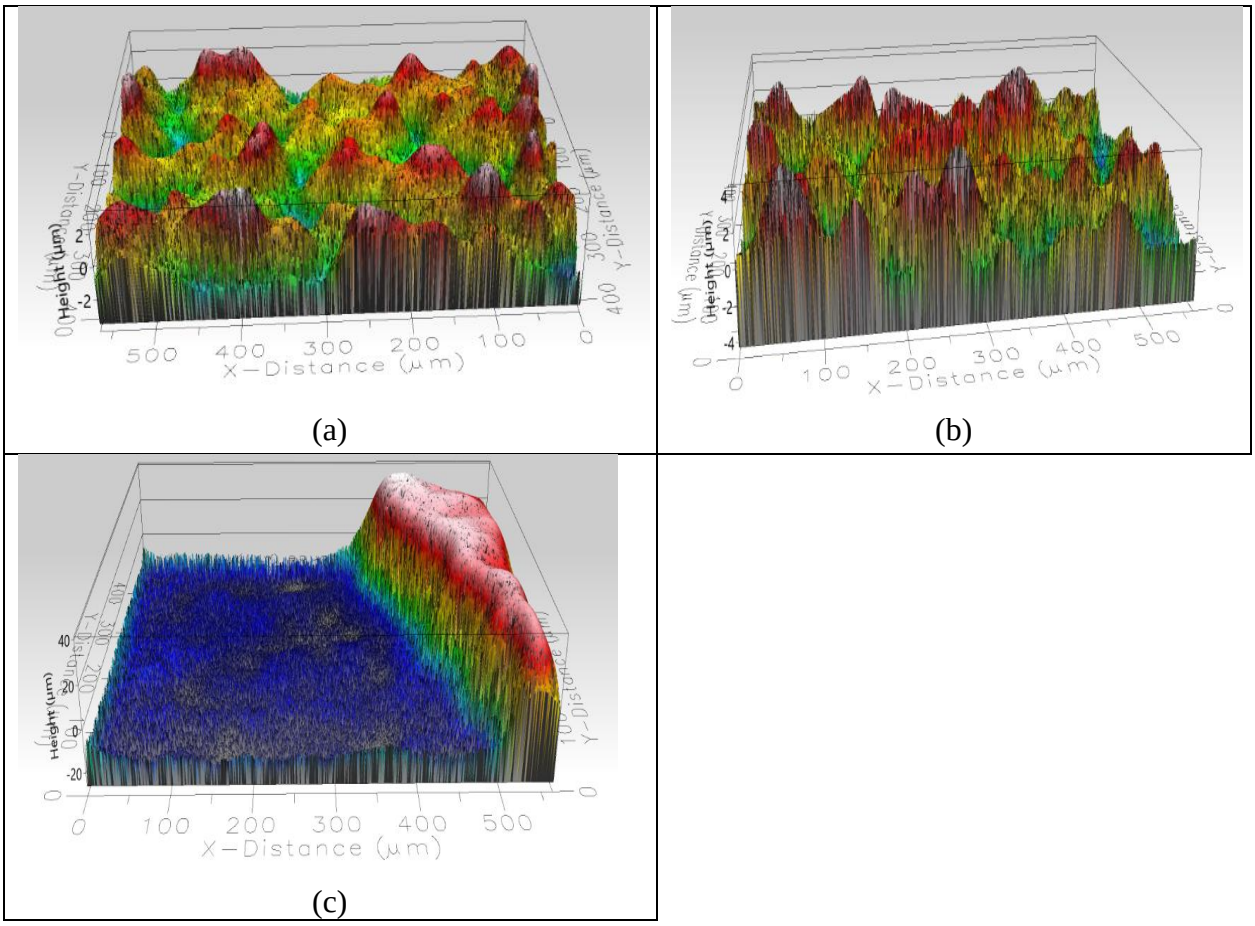

Figure 4. 19: Surface roughness scans acquired using profilometry of (a) Sylgard184 surface, (b) phosphor surface on Sylgard184 and (c) Sylgard184 phosphor boundary

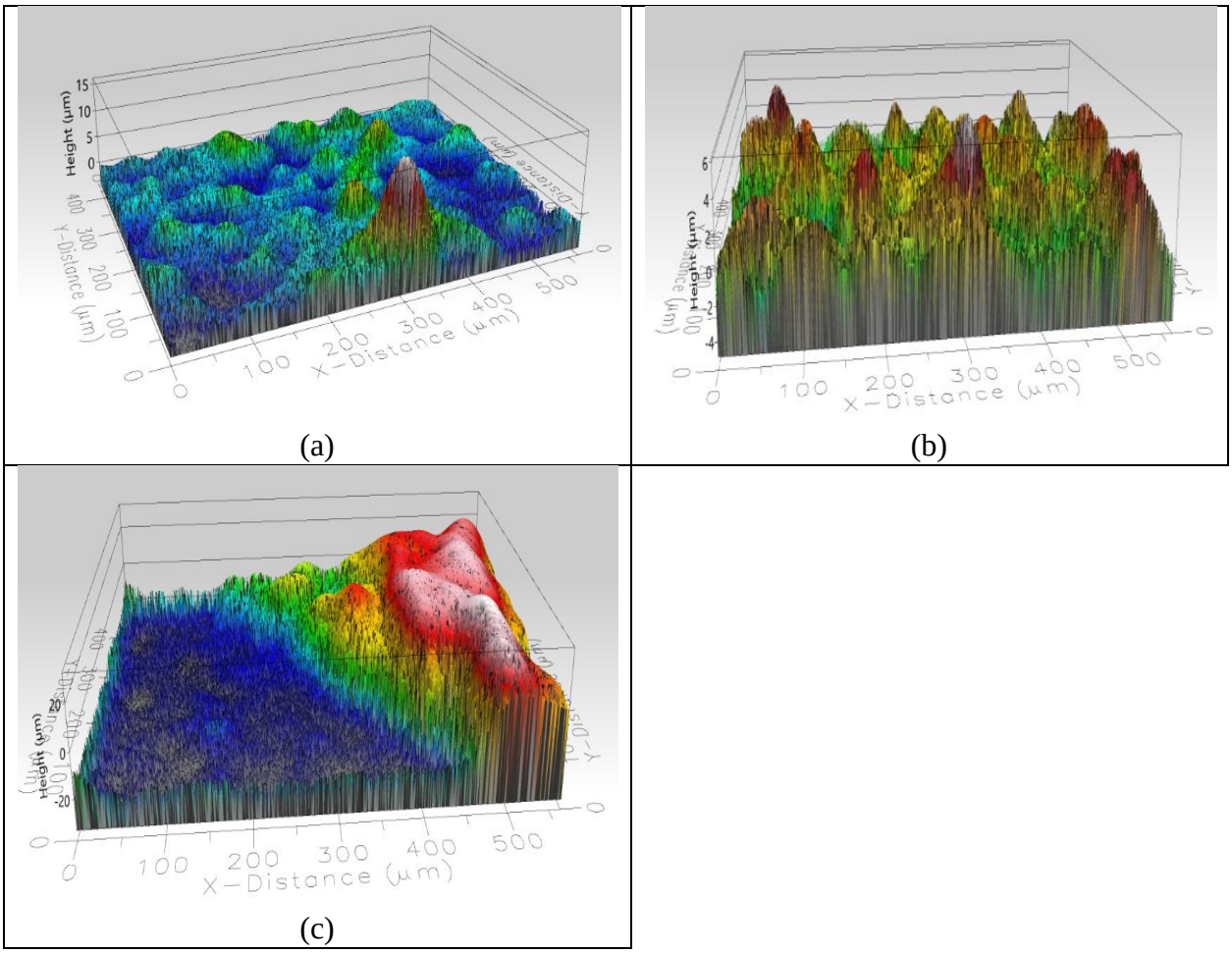

Figure 4.20: Surface roughness scans acquired using profilometry of (a) aerogel surface, (b) phosphor surface on aerogel and (c) aerogel phosphor boundary

Figure 4.19 a shows the Sylgard184 surface image. The average roughness height of this Sylgard184 surfaces was found to be 6.88 µm. Figure 4.19 b is the phosphor surface coated on sylgard184 and the average height was 8.87 µm. Similarly, Figure 4.19 c is the boundary of Sylgard184 and phosphor surface. This gives the information of the height of the coated phosphor on Sylgard184. This height was found to be 67.22 µm.

Figure 4.20 a is the surface image of aerogel only. The average roughness height was 20.47 µm. This data proves that the aerogel surface is rougher than Sylgard184. Figure 4.20 b is the just

phosphor surface on aerogel and it's height was 11.15 μm. Figure 4.20 c shows the phosphor aerogel boundary on aerogel surface. The height of the coated phosphor on aerogel was found to be 65.46 μm.

Chapter 5

Results: Temperature Dependent Luminescence of Flexible Ceramic Ribbons

While aerogels and elastomers have proven to be excellent media for encapsulation of thermographic phosphors both materials fail at temperatures above 400 ^{0}C. To accommodate applications that require a higher temperature of operation flexible ceramic sheets of 40 μm thick acquired from ENrG Inc were tested. This chapter summarizes the temperature dependent luminescence behavior of thermographs phosphors coated on flexible ceramic ribbons as a function of temperature.

5.1 Effect of ceramic ribbons on heat distribution

Initially, the maximum working temperature of Sylgard184 and silica aerogels directly in contact with the Instec heating stage was evaluated and used to establish the baseline. Material failure was defined as any detectable changes in the physical or chemical behavior of either material, whichever occurred first. In the case of Sylgard184, the assessment was classified as "material failure" at the onset of material releasing vapor and then followed by material cracking and fragmenting. In the case of the aerogel "material failure" was declared at the onset of discoloration which signified a chemical change. Each experiment for both materials was repeated three separate times and results reported here reflect the average values in each case. For Sylgard184, the vapor release occurred at 231 ^{0}C while crack formation and propagation occurred

at 354 ^{0}C. The results for aerogels in direct contact with the stage lead to the discovery of material failure at 270 ^{0}C at which point the experiment was halted.

To understand the effect of the ceramic ribbons on the performance of Sylgard184 and silica aerogels the number of ceramic ribbons underneath each material sample was increased from n=1 to n=3 and the maximum temperature of tolerance was evaluated. In brief, the maximum temperature of operation was increased in all cases delaying the temperature at which material failure would occur. The results are shown in Figure 5.1 and Figure 5.2 for Sylgard184 and silica aerogels respectively.

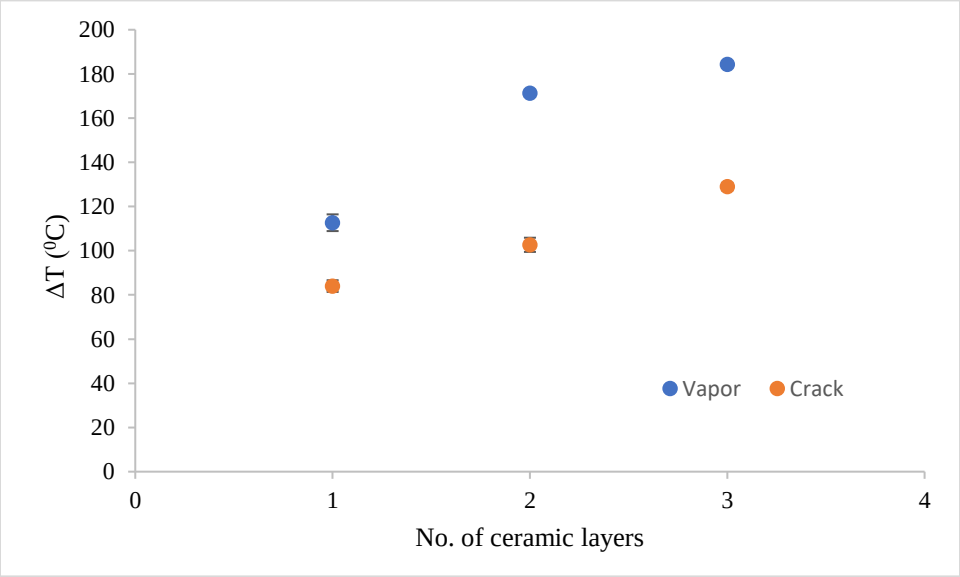

Figure 5.1: Graph of the number of ceramic layer vs. change in temperature (ΔT) due to ceramic layers for Sylgard184. Error bars reflect the standard deviation

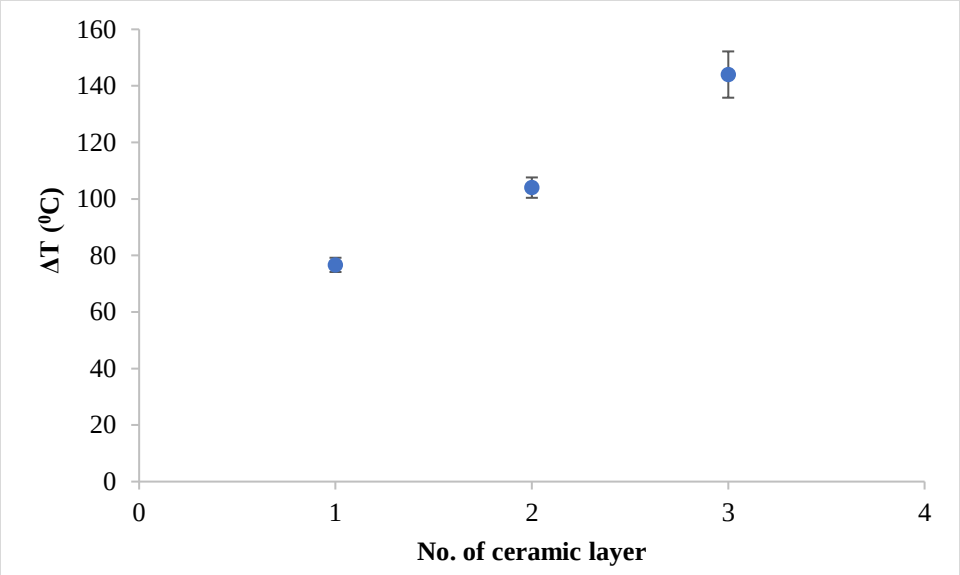

Figure 5.2: Graph of the number of ceramic layer vs. change in temperature (ΔT) due to ceramic layers for silica aerogel. Error bars reflect the standard deviation

For both materials, the first layer of the ceramic film increased the temperature of operation by at least 80 ^{0}C and had the biggest impact on the operating temperature. As seen in Figures 5.2 and 5.1 as the number of layers increases the temperature range of operation for both materials is extended in an (almost) linear fashion. For aerogels a total of 144 ^{0}C and for Sylgard184 a total of 110 ^{0}C extension in temperature of operation was accomplished by adding three (which is altogether 120 μm thin) layers.

The UV-Vis spectra of both materials were also evaluated before and after heating and shown here in Figure 5.3.

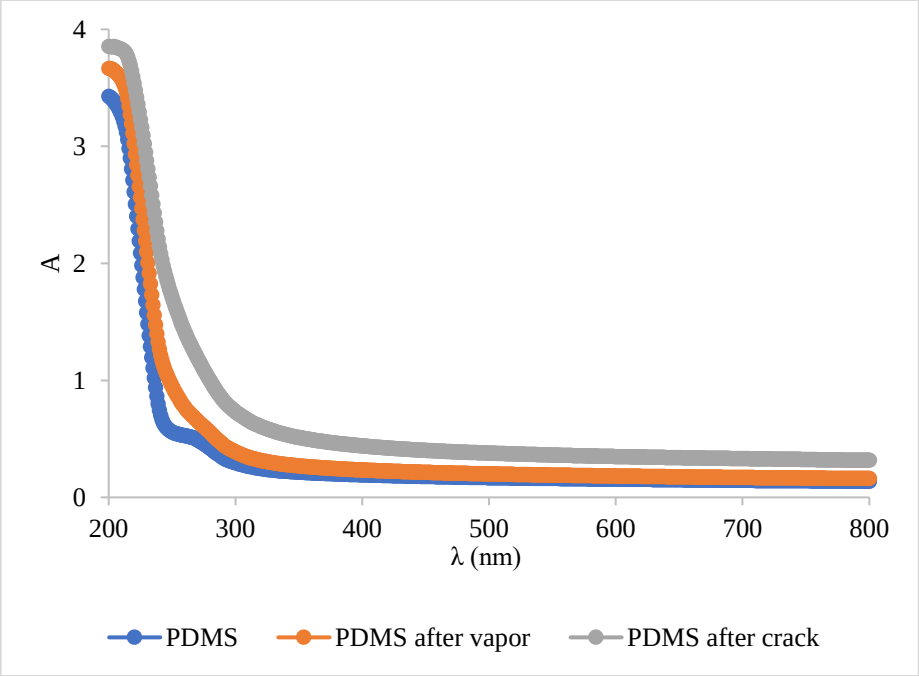
4
3
2
1
0
A
200
300
400
500
600
700
800
λ (nm)
PDMS
PDMS after vapor
PDMS after crack

(a)

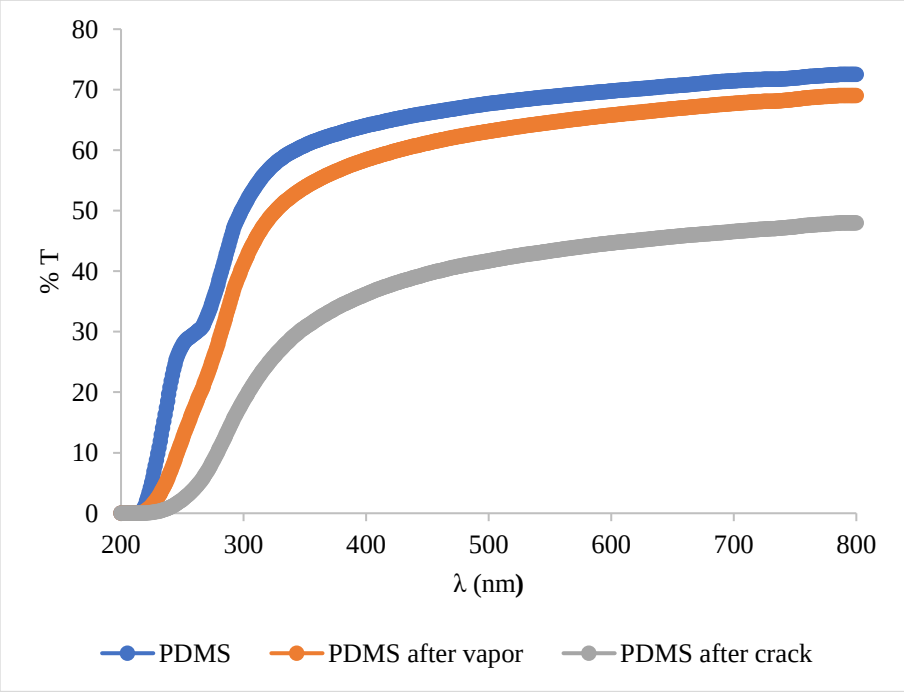
80
70
60
50
40
30
20
10
0
% T
200
300
400
500
600
700
800
λ (nm)
PDMS
PDMS after vapor
PDMS after crack

(b)

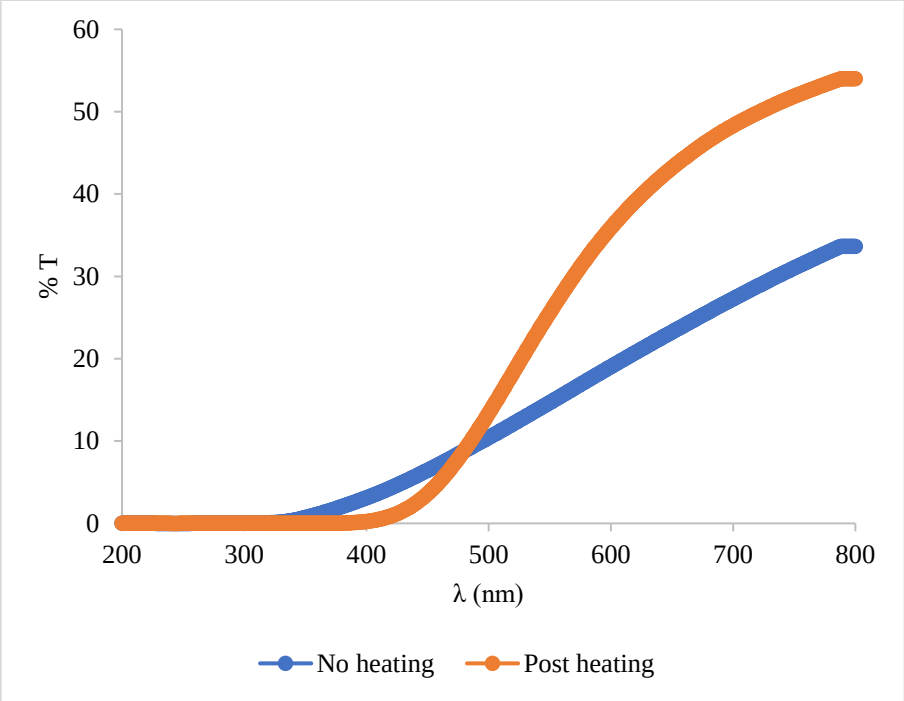

(c)

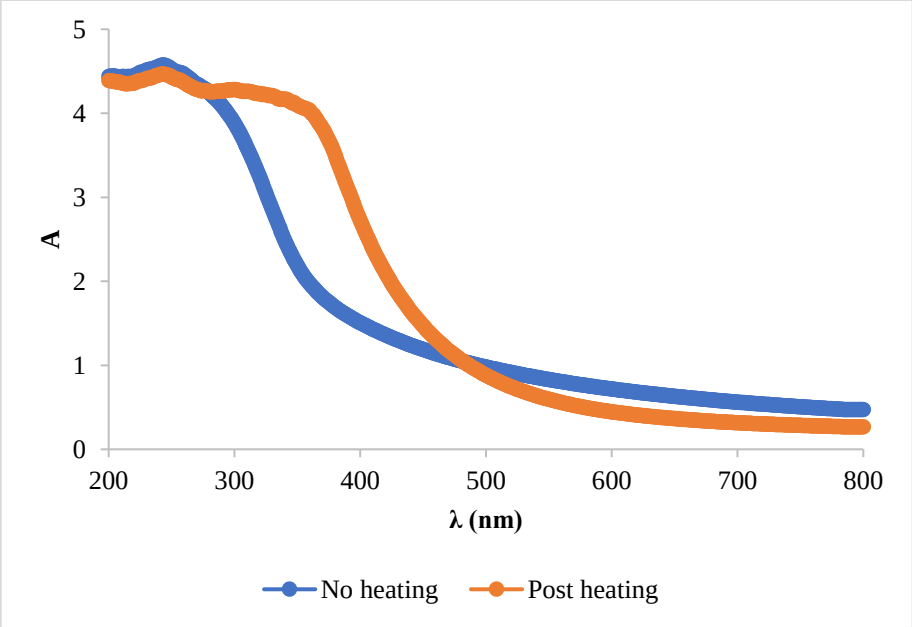

(d)

Figure 5.3: UV-Vis graph (a) % transmission (% T), (b) absorbance for Sylgard184 and, (c) % transmission (% T), (d) absorbance (A) for silica aerogel

In the case of Sylgard184 the appearance of cracks, as expected, affects the transparency of the material and as a result, the % T decreases post heating not only in the visible range but also in the UV range suggesting an advanced stage of material failure. For the aerogel samples, the degree of transmission increases post heating in the visible region.

5.2 Flexural strength of ceramic ribbons

The flexural strength of the ceramic ribbons was measured at three different temperatures; 400 ^{0}C, room temperature, and at -196 ^{0}C and results are shown in Figure 5.4 for all three temperatures. These temperatures reflect the range of applications that these materials might be expected to tolerate.

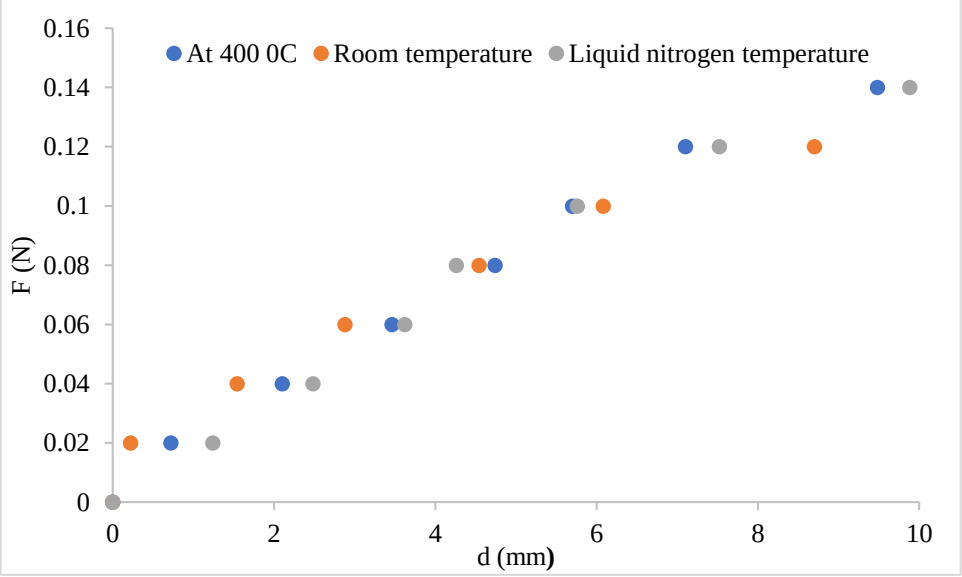

Figure 5.4: Flexural Strength: Force (F) vs. displacement (d) graph of the ceramic ribbons

The three-point bending tests were performed in the same manner and at the same rate for all three temperatures. A very small amount of difference in flexural strength was detected and is attributed to experimental error.

5.3 Heat distribution assessment on the ceramic sheet

An important analysis of the ceramic ribbons was to evaluate the heat distribution of the ceramics. This was accomplished by "Reading" the temperature at a set stage temperature at various points of the surface of the ceramic ribbon, using phosphor thermometry at four points. The points have been labeled as 1^{st}, 2^{nd}, 3^{rd}, and 4^{th} and results are shown in Table 5.1. Points 1 and 2 were located in the central region of the ribbon while points 3 and 4 were situated towards the edges of the ribbon. For each point, the luminescence was measured for 4 different temperatures: T_1= 216.63 ^{0}C, T_2=279.49 ^{0}C, T_3=398.42^{0}C and T_4= 505.46 ^{0}C and the corresponding decay times were calculated. The results of Table 5.1 are also presented in a graph form in Figure 5.5.

Table 5.1: Temperature distribution profile on ceramic ribbon

Stage temperature (^{0}C)	T (^{0}C) 1^{st} point (middle)	T (^{0}C) 2^{nd} point (middle)	T (^{0}C) 3^{rd} point (edge)	T (^{0}C) 4^{th} point (edge)
216.63	160.56	162.26	179.25	180.95
279.49	213.23	213.23	221.72	220.03
398.42	342.35	338.96	350.85	357.64
505.46	496.96	496.96	503.76	503.76

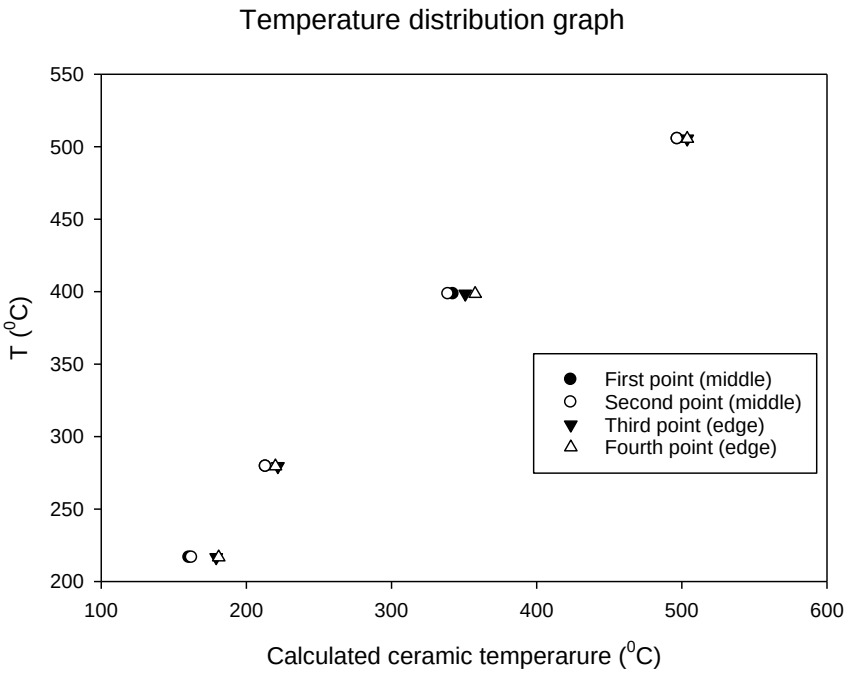

Figure 5.5: Graph showing the temperature distribution on the ceramic sheet

These results show that there is a significant temperature difference between the central points and an edge region(s) with the edges showing a higher temperature. This difference in temperature is more significant at lower temperatures.

5.4 Temperature dependent luminescence

Siloxane based polymers and silica aerogels are versatile materials that are used in a variety of industries from aerospace to biomedical needs [43], [45], [46]. As demonstrated these materials cannot tolerate excessively high temperatures and the use of a temperature buffering layer such as ceramic ribbons would be necessary in some cases. Here, the temperature dependent luminescence of several phosphors was tested after being coated on a ceramic ribbon and compared with the behavior of the phosphors when they were directly placed on the heating stage which served as the control.

Results for Gd_2O_2S: Eu phosphor-ceramic composite and YAG: Dy phosphor-ceramic composite are shown in Figure 5.6 for a range of temperatures starting at 200 ^{0}C and as high as 1039 ^{0}C.

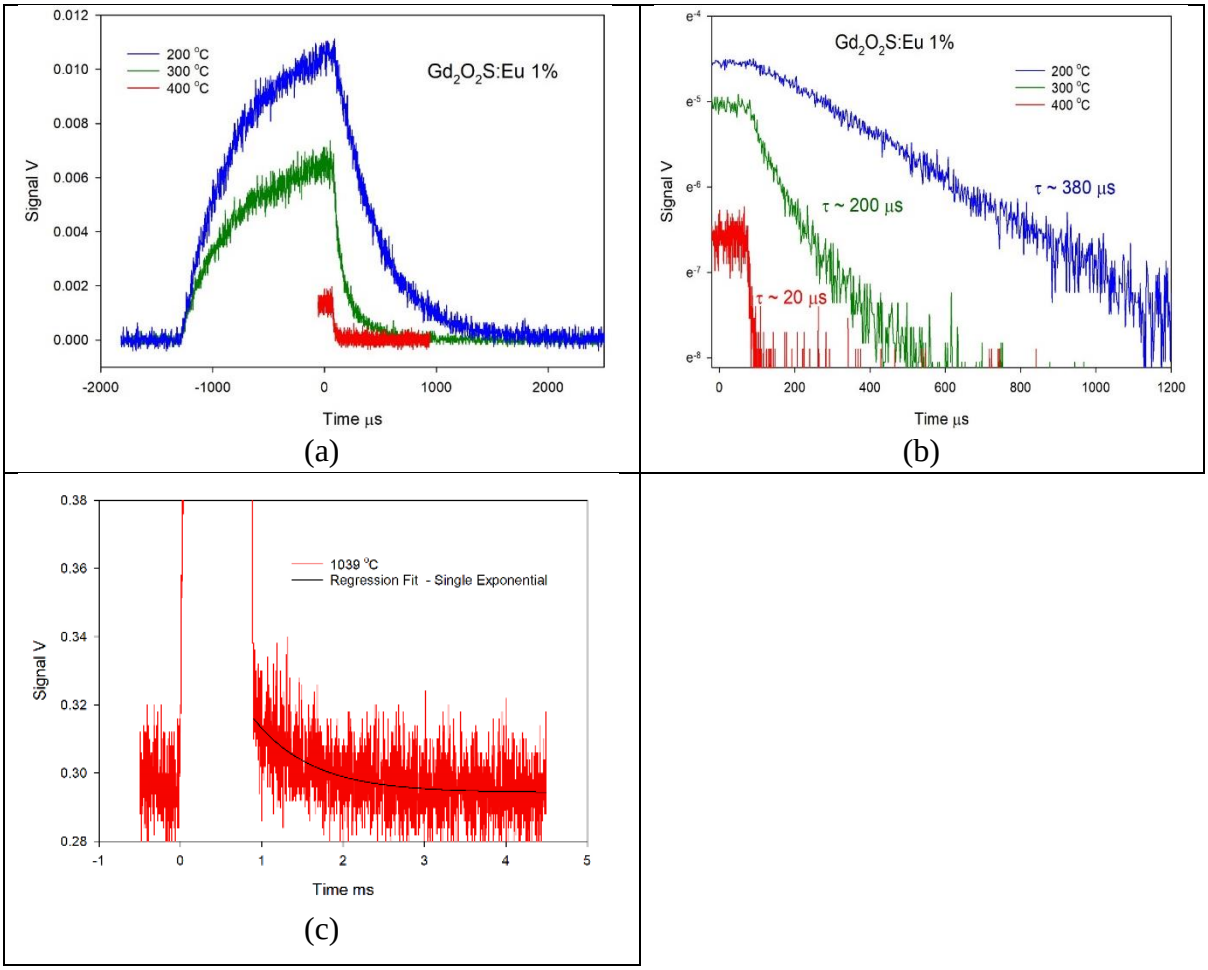

Figure 5.6: Plot of (a) signal voltage with time (b) log of signal voltage with time to find decay time of Gd_2O_2S: Eu/ceramic composite and (c) signal voltage vs time with a regression fit for YAG: Dy/ceramic composites at 1039 ^{0}C

Figure 5.6 a shows the detected phosphorescence signal at 200 ^{0}C, 300 ^{0}C and 400 ^{0}C for the Gd_2O_2S: Eu phosphor coated on ceramic. This temperature dependent signal along with decay time shows the feasibility of using the phosphor-ceramic composite for thermometry. Figure 5.6 b is the log of signal voltage vs time graph providing decay time information. YAG: Dy phosphor-

ceramic composite was used to study luminescence above 400 ^{0}C. Since the Gd_2O_2S: Eu phosphor did not show strong intensity –based temperature dependent luminescence at high temperatures above 400 ^{0}C. Figure 5.6 c shows the luminescence decay curve at 1039 ^{0}C for YAG: Dy phosphor-ceramic composite with a decay time of 715 μs corresponding to the set temperature.

Chapter 6

Conclusion and Future Recommendations

Silica aerogels were successfully patterned with an array of phosphor patches in an off-axis pattern and tested as a function of temperature. The main goal of the study was to not only establish the methodology for preparing reproducibly aerogel+ phosphor patterned array samples, but also to interrogate the opposite side of the aerogel substrate as a function of temperature. This was an important part of the study since the structure created here has the potential to be used as a heat flux measurement device. This meant that the excitation and the emission signals had to travel through the entire thickness of the aerogel material when interrogating the opposite side of the aerogel. This is challenging due to the mesoporous nature of the aerogels and the significant amount of scatter that occurs as light travels through the material. With the optical setup used in this study a maximum aerogel thickness of 6.5 mm was successfully tested meaning that accurate temperature information was inferred from the side that was 6.5 mm away from the point of entry of the excitation signal. It might be possible to gather temperature information from samples thicker than 6.5 mm with a different set of optical components and laser, and with a different phosphor compound but was not in the scope of this study.

The patterning technique used here was rather crude and only for the purpose of feasibility study. For future studies a more refined method needs to be developed such that smaller and more well-defined patches can be created.

Sylgard184 samples prepared in this study served as a control and results from the aerogels were compared with results of similar structures created in Sylgard184. As expected the excitation/

emission signals were not noticeably attenuated as a result of travelling through Sylgard184 samples of increasing thicknesses.

In both cases, Sylgard184 and silica aerogels' thermal expansion was neglected and not taken into consideration when heat flux was calculated. While this does cause an error in the calculation, it is negligible in the temperature range that was investigated in this study. Another source of error that was also ignored was the contact area of the phosphor patches with the heating/ cooling stages that were used to ramp the substrate temperature. Surface profilometry showed non-uniformities in the phosphor patch regions that might cause uneven heating of the phosphor particles which were used for calculating temperature. This however is not expected to have a significant contribution to the measurements reported here since it is beyond the resolution of the equipment used to conduct this study.

To increase the temperature range of operation of both silica aerogels and Sylgard184 a heat buffer would be necessary. In this study preliminary tests were performed to evaluate the feasibility of flexible ceramic ribbons on maximum temperature of operation of the materials of interest. A single layer of a 40 μm ceramic ribbon extended the temperature of operation by at least 100 ^{0}C and more as the number of layers increased. In future work will be done to find ways to incorporate these ribbons into the synthesis protocol.

References

[1] J. G. Webster, “The Measurement, Instrumentation and Sensors Handbook,” p. 2588, 1999.

[2] K. E. Mitchell, V. Gardner, S. W. Allison, and F. Sabri, “Synthesis and characterization of flexible thermographic phosphor temperature sensors,” *Opt. Mater.*, vol. 60, pp. 50–56, 2016.

[3] “Automatic Pyrometers,” in *Temperature Measurement*, Wiley-Blackwell, 2002, pp. 177–208.

[4] P. Parajuli, S. W. Allison, and F. Sabri, “Spincoat-fabricated multilayer PDMS-phosphor composites for thermometry,” *Meas. Sci. Technol.*, vol. 28, no. 6, p. 065101, 2017.

[5] S. W. Allison and G. T. Gillies, “Remote thermometry with thermographic phosphors: Instrumentation and applications,” *Rev. Sci. Instrum.*, vol. 68, no. 7, pp. 2615–2650, Jul. 1997.

[6] B. Atakan, C. Eckert, and C. Pflitsch, “Light emitting diode excitation of Cr 3+ :Al 2 O 3 as thermographic phosphor: experiments and measurement strategy,” *Meas. Sci. Technol.*, vol. 20, no. 7, p. 075304, 2009.

[7] F. Sabri, J. Marchetta, and K. M. Smith, “Thermal conductivity studies of a polyurea cross-linked silica aerogel-RTV 655 compound for cryogenic propellant tank applications in space,” *Acta Astronaut.*, vol. 91, pp. 173–179, Oct. 2013.

[8] R. S. Fontenot, S. W. Allison, K. J. Lynch, W. A. Hollerman, and F. Sabri, “Mechanical, spectral, and luminescence properties of ZnS:Mn doped PDMS,” *J. Lumin.*, vol. 170, pp. 194–199, Feb. 2016.

[9] P. Pringsheim, “Fluorescence and Phosphorescence (Interscience, New York, 1949),” *Google Sch.*, p. 349, 1990.

[10] “Luminescence and the Solid State, Volume 12 - 1st Edition.” [Online]. Available: https://www.elsevier.com/books/luminescence-and-the-solid-state/ropp/978-0-444-88940-9. [Accessed: 02-Jul-2018].

[11] N. Paul, “Device for indicating the temperature distribution of hot bodies,” US2071471A, 23-Feb-1937.

[12] “A Temperature-Sensitive Phosphor Used to Measure Surface Temperatures in Aerodynamics: Review of Scientific Instruments: Vol 24, No 3.” [Online]. Available: https://aip.scitation.org/doi/abs/10.1063/1.1770668. [Accessed: 18-Jul-2018].

[13] K. A. James, W. H. Quick, and V. H. Strahan, “FIBER OPTICS-WAY TO TRUE DIGITAL SENSORS,” *Control Eng.*, vol. 26, no. 2, pp. 30–33, 1979.

[14] K. W. Tobin, S. W. Allison, M. R. Cates, G. J. Capps, and D. L. Beshears, “High-temperature phosphor thermometry of rotating turbine blades,” *AIAA J.*, vol. 28, no. 8, pp. 1485–1490, Aug. 1990.

[15] S. Allison, A. Hollerman, M. Cates, T. Bencic, J. Eldridge, and C. Mercer, “Advances in High Temperature Phosphor Thermometry for Aerospace Applications,” in *39th AIAA/ASME/SAE/ASEE Joint Propulsion Conference and Exhibit*, American Institute of Aeronautics and Astronautics.

[16] A. Omrane, F. Ossler, M. Alden, U. Gtoransson, and G. Holmstedt, “Surface Temperature Measurement Of Flame Spread Using Thermographic Phosphors,” *Fire Saf. Sci.*, vol. 7, pp. 141–152, 2003.

[17] S. Alaruri, T. Bonsett, A. Brewington, E. McPheeters, and M. Wilson, “Mapping the surface temperature of ceramic and superalloy turbine engine components using laser-induced fluorescence of thermographic phosphor,” *Opt. Lasers Eng.*, vol. 31, no. 5, pp. 345–351, 1999.
[18] R. L. Vander Wal, P. A. Householder, and T. W. Wright, “Phosphor thermometry in combustion applications,” *Appl. Spectrosc.*, vol. 53, no. 10, pp. 1251–1258, 1999.
[19] T. E. Diller and S. Onishi, “Heat flux gage,” US4779994A, 25-Oct-1988.
[20] A. H. Epstein, G. R. G. Jr, and R. J. G. Norton, “High frequency response multilayer heat flux gauge configuration,” US4722609A, 02-Feb-1988.
[21] M. Hayashi, A. Sakurai, and S. Aso, “Multi-layered thin film heat transfer gauge,” US4577976A, 25-Mar-1986.
[22] B. W. Noel, H. M. Borella, M. R. Cates, W. D. Turley, C. D. MacArthur, and G. C. Cala, “Optical heat flux gauge,” US5005984A, 09-Apr-1991.
[23] P. Tsou, “Silica aerogel captures cosmic dust intact,” *J. Non-Cryst. Solids*, vol. 186, pp. 415–427, 1995.
[24] D. M. Smith, A. Maskara, and U. Boes, “Aerogel-based thermal insulation,” *J. Non-Cryst. Solids*, vol. 225, pp. 254–259, 1998.
[25] S. M. Jones, “Aerogel: space exploration applications,” *J. Sol-Gel Sci. Technol.*, vol. 40, no. 2–3, pp. 351–357, 2006.
[26] W. M. Rohsenow, J. P. Hartnett, and Y. I. Cho, Eds., *Handbook of heat transfer*, 3rd ed. New York: McGraw-Hill, 1998.
[27] “Introduction to Heat Transfer, 6th Edition,” *Wiley.com*. [Online]. Available: https://www.wiley.com/en-us/Introduction+to+Heat+Transfer%2C+6th+Edition-p-9780470501962. [Accessed: 24-May-2018].
[28] “An Instrument for the Direct Measurement of Intense Thermal Radiation: Review of Scientific Instruments: Vol 24, No 5.” [Online]. Available: https://aip.scitation.org/doi/abs/10.1063/1.1770712. [Accessed: 05-Jun-2018].
[29] A. H. Khalid and K. Kontis, “Thermographic Phosphors for High Temperature Measurements: Principles, Current State of the Art and Recent Applications,” *Sensors*, vol. 8, no. 9, pp. 5673–5744, Sep. 2008.
[30] N. Fuhrmann, J. Brübach, and A. Dreizler, “Phosphor thermometry: A comparison of the luminescence lifetime and the intensity ratio approach,” *Proc. Combust. Inst.*, vol. 34, no. 2, pp. 3611–3618, Jan. 2013.
[31] “Comparison of fluorescence-based temperature sensor schemes: Theoretical analysis and experimental validation: Journal of Applied Physics: Vol 84, No 9.” [Online]. Available: https://aip.scitation.org/doi/abs/10.1063/1.368705. [Accessed: 29-May-2018].
[32] D. J. E. Parks, “Temperature Dependent Lifetime Measurements of Fluorescence from a Phosphor,” p. 22.
[33] R. H. Krauss, R. G. Hellier, and J. C. McDaniel, “Surface temperature imaging below 300 K using La_2O_2S:Eu,” *Appl. Opt.*, vol. 33, no. 18, pp. 3901–3904, Jun. 1994.
[34] M. R. Cates, D. L. Beshears, S. W. Allison, and C. M. Simmons, “Phosphor thermometry at cryogenic temperatures,” *Rev. Sci. Instrum.*, vol. 68, no. 6, pp. 2412–2417, Jun. 1997.
[35] J. Brübach, A. Dreizler, and J. Janicka, “Gas compositional and pressure effects on thermographic phosphor thermometry,” *Meas. Sci. Technol.*, vol. 18, no. 3, p. 764, 2007.
[36] L. Thorington, “Temperature Dependence of the Emission of an Improved Manganese-Activated Magnesium Germanate Phosphor,” *JOSA*, vol. 40, no. 9, pp. 579–583, Sep. 1950.

[37] W. M. Yen, S. Shionoya, and H. Yamamoto, “Phosphor Handbook CRC Press,” *Boca Raton*, 2007.
[38] J. Zhao *et al.*, “Single-nanocrystal sensitivity achieved by enhanced upconversion luminescence,” *Nat. Nanotechnol.*, vol. 8, no. 10, pp. 729–734, Oct. 2013.
[39] J. R. Lakowicz, “Introduction to Fluorescence,” in *Principles of Fluorescence Spectroscopy*, Springer, Boston, MA, 1999, pp. 1–23.
[40] M. Sauer, J. Hofkens, and J. Enderlein, *Handbook of Fluorescence Spectroscopy and Imaging: From Ensemble to Single Molecules*. John Wiley & Sons, 2010.
[41] J. R. Askim, M. Mahmoudi, and K. S. Suslick, “Optical sensor arrays for chemical sensing: the optoelectronic nose,” *Chem. Soc. Rev.*, vol. 42, no. 22, pp. 8649–8682, Oct. 2013.
[42] H. D. Gesser and P. C. Goswami, “Aerogels and related porous materials,” *Chem. Rev.*, vol. 89, no. 4, pp. 765–788, Jun. 1989.
[43] P. Parajuli, S. W. Allison, and F. Sabri, “Spincoat-fabricated multilayer PDMS-phosphor composites for thermometry,” *Meas. Sci. Technol.*, vol. 28, no. 6, p. 065101, 2017.
[44] Y. Yang *et al.*, “Optical thermometry based on the upconversion fluorescence from Yb3+/Er3+ codoped La2O2S phosphor,” *Ceram. Int.*, vol. 40, no. 7, Part A, pp. 9875–9880, Aug. 2014.
[45] F. Sabri, J. Marchetta, and K. M. Smith, “Thermal conductivity studies of a polyurea cross-linked silica aerogel-RTV 655 compound for cryogenic propellant tank applications in space,” *Acta Astronaut.*, vol. 91, pp. 173–179, Oct. 2013.
[46] F. Sabri, J. A. Cole, M. C. Scarbrough, and N. Leventis, “Investigation of Polyurea-Crosslinked Silica Aerogels as a Neuronal Scaffold: A Pilot Study,” *PLOS ONE*, vol. 7, no. 3, p. e33242, Mar. 2012.